COOPERATIVE SPONTANEOUS EMISSION FROM VOLUME SOURCES IN LAYERED MEDIA

ENRICO NICHELATTI

ENEA - Dipartimento Tecnologie Fisiche e Nuovi Materiali
Centro Ricerche Casaccia, Roma

RT/2009/4/FIM

ENTE PER LE NUOVE TECNOLOGIE,
L'ENERGIA E L'AMBIENTE

COOPERATIVE SPONTANEOUS EMISSION FROM VOLUME SOURCES IN LAYERED MEDIA

ENRICO NICHELATTI

ENEA - Dipartimento Tecnologie Fisiche e Nuovi Materiali
Centro Ricerche Casaccia, Roma

RT/2009/4/FIM

COOPERATIVE SPONTANEOUS EMISSION FROM VOLUME SOURCES IN LAYERED MEDIA

ENRICO NICHELATTI

Abstract
The classical theory of radiation from a dipole located inside a microcavity is extended to the case of a volume source placed inside a layered medium. Cooperation phenomena that can take place in the spontaneous emission process are taken into account with an approach based on the theory of spatial coherence. Three cases are considered: non-cooperation, long-range cooperation, and short-range cooperation. In all these cases, the expressions found for the outcoupled power are analytical.
As an application of the theory, an Alq_3-based organic light emitting diode is analyzed. The optical properties of the device are evaluated and compared for two different types of cathode, one consisting of an Al layer, the other one consisting of an Al/LiF bi-layer. The results found show that the ultra-thin LiF layer significantly improves extraction efficiency.

Keywords: *spontaneous emission, cooperative spontaneous emission, spatial coherence, volume source, layered medium, optical microcavity, organic light emitting diode*

EMISSIONE SPONTANEA COOPERATIVA DA SORGENTI ESTESE IN MEZZI STRATIFICATI

Riassunto
La teoria classica dell'emissione luminosa da parte di un dipolo in microcavità è generalizzata al caso di una sorgente estesa in un mezzo striato. Sono presi in considerazione fenomeni di cooperazione nel processo di emissione spontanea partendo dalla teoria della coerenza spaziale. Sono considerati tre casi: assenza di cooperazione, cooperazione a lungo raggio e cooperazione a corto raggio. In tutti questi casi, le espressioni trovate per la potenza accoppiata esternamente sono analitiche.
Come applicazione della teoria, viene analizzato un diodo organico emettitore di luce basato su Alq_3. Le proprietà ottiche del dispositivo sono calcolate e messe a confronto per due differenti tipi di catodo, uno consistente in uno strato di Al, l'altro consistente in un bi-strato Al/LiF. I risultati trovati mostrano che lo strato ultra-sottile di LiF migliora sensibilmente l'efficienza di estrazione.

Parole chiave: emissione spontanea, emissione spontanea cooperativa, coerenza spaziale, sorgente estesa, mezzo striato, microcavità ottica, diodo organico emettitore di luce

Contents

1 Introduction

Spontaneous emission (SpE) is one of the most noticeable manifestations of the interaction of matter with vacuum: fluctuations of the electromagnetic vacuum field can induce an atomic system to decay to its ground state with the emission of photons [1,2]. For this reason, SpE is often regarded as being stimulated by a *virtual photon* [1,2]. In this framework, any alteration of the vacuum-field modes results in the modification of the SpE properties of atomic systems. In particular, the SpE rate can be enhanced or inhibited by vacuum-field modes.

A planar optical cavity, that is, a portion of space confined within two mirrors, is perhaps the easiest way to locally alterate vacuum-field modes [2]. Purcell conjectured for the first time how the SpE rate of atomic systems could be altered by the local density of electromagnetic modes in a small resonator of such a kind [3]. Since then, many works have contributed to gain more and more insight into Purcell's intuition [4–21].

Atoms or molecules can coherently interact in the SpE process, with noticeable effects on the decay rate and radiated electromagnetic field. The first studies in this field date back to 1954, when Dicke studied cooperative SpE phenomena in a gas also introducing the concept of superradiance [22]. After that, other studies on the subject were published including the effects of single mirrors, optical traps and cavities on the coherent interaction among the emitters [23–31].

Coherent interaction among single elements of a volume source and its dependence on their mutual distances is a well known topic in spatial coherence theory [32–34]. Although spatial coherence theory could represent a complementary approach to the study of cooperative phenomena, very few works can be found that adopt it to evaluate SpE characteristics in a planar microcavity [35]. In Ref. 35, a Green's function approach is used to that purpose. To the best of the author's knowledge, an approach relying on classical multireflections and the effect on them of spatial coherence of a volume source has never been published.

In the present report, a theoretical model based on the classical theory of spatial coherence is developed to evaluate the angular distribution of power radiated from a volume source embedded in a layered medium. To that purpose, a classical model for the emission from a point source in a planar structure [16,17] is generalized with the introduction of coherent interaction of each point of the volume source with other points that are found within a certain spatial range. The model is not meant to explain why and how separated points of the source can coherently interact; rather, the interaction is assumed to be of spatially-coherent nature so that one can evaluate how the radiated power changes with respect to that radiated by a single point source. It is shown how particular forms of the complex degree of coherence of the source—such as a three-dimensional Gaussian function—can lead to analytical results. A few examples are given and discussed.

As an application of the model, an Alq_3-based organic light-emitting diode (OLED) is theoretically inspected to evaluate how different configurations of the cathode—single Al layer or Al/LiF bi-layer—influence its electroluminescence properties.

The present report is organized as follows.

In Sec. 2, a classical model for the emission from a point source in a planar structure [16, 17] is reviewed and adapted to the notation and conventions here adopted. An example is given with an elementary microcavity formed by mirrors that are ideally independent from polarization and incidence-angle.

In Sec. 3, the above-mentioned classical model is generalized to a volume source. Three possible cases are assumed for the coherent interaction among elementary components of the source: no

interaction at all, the ideal case of full (long-range) interaction, and the more realistic case of range-dependent interaction. In the last case, the core of the theoretical model is developed on the basis of the theory of spatial coherence and the concept of complex degree of coherence. A few examples are given for the same elementary microcavity of Sec. 2.

In Sec. 4, two configurations of an Alq_3-based OLED are modeled by assuming alternatively absence of cooperation and short-range cooperation among the Alq_3 molecules. A three-dimensional Gaussian function is chosen to represent the complex degree of coherence. With both approaches, which lead to analytical expressions, the use of an Al/LiF cathode in place of a simpler Al cathode is demonstrated to significantly improve the extraction efficiency of the device.

Conclusions are eventually drawn and discussed in Sec. 5.

2 Point source in a layered medium

The simplest case to analyze consists probably in a single atomic system sandwiched between two mutually parallel plane mirrors. These mirrors can be single metal layers, distributed Bragg reflectors, or multilayers of any kind. The atomic system, being much smaller in size than the emission wavelength, behaves like a point source and can be modeled as if it were a randomly-oriented elementary dipole. As will be shown in the following, the random orientation of the dipole can be dealt with a suitable superposition of basic orientation and polarization states.

To describe radiation from an elementary dipole, one can introduce *ad hoc* electric-field source terms [16, 17]. For a dipole that lies horizontally (h) with respect to the medium layering, the source terms are four,

$$A_{\uparrow}^{(h),s} \equiv A_{\downarrow}^{(h),s} = \sqrt{\frac{3}{16\pi}}\,, \qquad A_{\uparrow}^{(h),p} \equiv A_{\downarrow}^{(h),p} = \sqrt{\frac{3}{16\pi}}\cos\theta_0\,, \tag{2.1}$$

where s and p stand for the polarization state and the arrows in the subscripts indicate the emission direction—upwards ($\uparrow$) or downwards ($\downarrow$). The angle θ_0 is measured *within* the central medium[1] and with respect to the normal direction in such a way that its value is $\theta_0 = 0$ both for normally upward and downward emission. See Fig. 1 for a scheme of the cavity with symbols and conventions used. The units of the source terms are those of an electric field, that is, Vm^{-1} in the MKSA system. For a vertically (v) oriented dipole, the non-zero source terms are only two,

$$A_{\uparrow}^{(v),p} \equiv -A_{\downarrow}^{(v),p} = \sqrt{\frac{3}{8\pi}}\sin\theta_0\,, \tag{2.2}$$

being $A_{\uparrow}^{(v),s} = A_{\downarrow}^{(v),s} = 0$.

The above-defined source terms represent the amplitudes of the electric fields radiated by the dipole in the host material—however, their dependence on the observation distance is neglected for simplicity—and are used to evaluate the amplitude of the electric fields that are outcoupled in the far field in the external medium, in the top ($\uparrow$) and bottom ($\downarrow$) half-space, respectively, as [16, 17]

$$E_{\uparrow\downarrow} = \tau_{\uparrow\downarrow}\frac{A_{\uparrow\downarrow} + \rho_{\downarrow\uparrow}A_{\downarrow\uparrow}}{1 - \rho_{\uparrow}\rho_{\downarrow}}\,. \tag{2.3}$$

[1] The angle of propagation has to comply with Snell's law of refraction when light crosses borders of media with different optical constants [33].

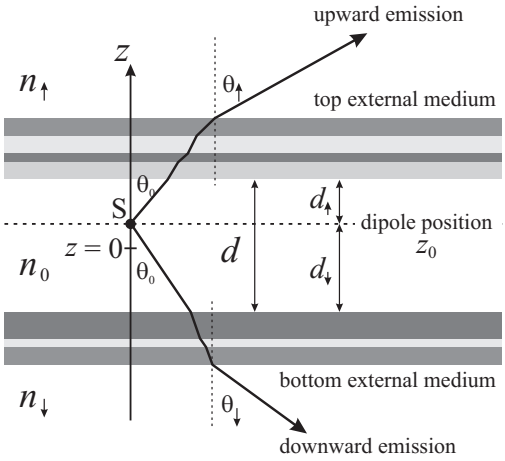

Figure 1. Scheme of a single point source in a cavity. The point source, S, is embedded in a medium of refractive index n_0 and thickness d and is surrounded by two mutually parallel multilayers. The whole cavity is placed inside an external medium, whose top and bottom parts have refractive indices $n_\uparrow$ and $n_\downarrow$, respectively. The dipole is placed at $z = z_0$, being $z = 0$ the centre of the internal medium. The distances of the dipole from the top and bottom mirror are $d_\uparrow$ and $d_\downarrow$, respectively. The propagation angles, θ_0 and $\theta_{\uparrow\downarrow}$, are measured with respect to the normal, both for upwards (↑) and downwards (↓) emission. For simplicity, multiple internal reflections are not shown in the figure.

Here and in the following, the double-arrow subscript is a compact form to represent two equations in one, one for the first arrow, the other for the second one. In Eq. (2.3), $\tau_\uparrow$ and $\rho_\uparrow$ ($\tau_\downarrow$ and $\rho_\downarrow$) are the complex-amplitude transmittance and reflectance, respectively, of the space interval that exists between the dipole and the top (bottom) half-space. Such coefficients depend on both angle and polarization state [36–38].[2] Hereafter, the superscripts corresponding to dipole orientation and polarization state are used also for the electric fields and outcoupled powers, *e.g.*, $E_{\uparrow\downarrow}^{(h),s}$ indicates the amplitude of the s-polarized electric field component that is generated by a horizontal dipole having $A_{\uparrow\downarrow}^{(h),s}$ as source terms. However, they are omitted whenever the equations hold true for any orientation and polarization state, like in Eq. (2.3).

Let us assume that external top and bottom half spaces have real refractive indices $n_\uparrow$ and $n_\downarrow$, respectively. Let n_0 be the refractive index of the medium the dipole is embedded in. In the following, for simplicity n_0 will be taken to be a real quantity, but the theory can be straightforwardly generalized to the case of complex n_0. Because $E_{\uparrow\downarrow}$ represents the amplitude of a transmitted electric field[3] with complex-amplitude transmittance $\tau_{\uparrow\downarrow}$, the laws of intensity transmission through a multilayer apply [36–38] and the outcoupled polarized power components of a dipole are, apart from unessential common factors,

$$w_{\uparrow\downarrow}^s = \frac{n_{\uparrow\downarrow}\cos\theta_{\uparrow\downarrow}}{\cos\theta_0}\left|E_{\uparrow\downarrow}^s\right|^2, \qquad w_{\uparrow\downarrow}^p = \frac{n_{\uparrow\downarrow}\cos\theta_0}{\cos\theta_{\uparrow\downarrow}}\left|E_{\uparrow\downarrow}^p\right|^2, \tag{2.4}$$

which are valid for any orientation , (h) or (v).

[2] As one could expect, Eq. (2.3) is true also for a single dipole in vacuum, provided the substitutions $\tau_{\uparrow\downarrow} = \exp(\mathrm{i}\phi_{\uparrow\downarrow})$ and $\rho_{\uparrow\downarrow} = 0$ are applied, where $\phi_{\uparrow\downarrow}$ is an arbitrary phase term.

[3] Whose amplitude before transmission is

$$\frac{A_{\uparrow\downarrow} + \rho_{\downarrow\uparrow}A_{\downarrow\uparrow}}{1 - \rho_\uparrow\rho_\downarrow}.$$

The above equations are true for plane waves. However, here we are considering spherical waves that are originated from a point source and detected in the far field. A correction to take into account how finite solid angles change on refraction is therefore needed [16, 17, 39]. Such a correction is derived in Appendix A and results in the multiplicative factor $\frac{n_{\uparrow\downarrow}^2 \cos\theta_{\uparrow\downarrow}}{n_0^2 \cos\theta_0}$ for the outcoupled power components. These become

$$w_{\uparrow\downarrow}^s = \frac{n_{\uparrow\downarrow}^3 \cos^2\theta_{\uparrow\downarrow}}{n_0^2 \cos^2\theta_0} \left|E_{\uparrow\downarrow}^s\right|^2, \qquad w_{\uparrow\downarrow}^p = \frac{n_{\uparrow\downarrow}^3}{n_0^2} \left|E_{\uparrow\downarrow}^p\right|^2. \tag{2.5}$$

Again, the equations are suitable for any orientation.

Now, let d be the thickness of the layer the elementary dipole is embedded in, and let $d_\uparrow$ and $d_\downarrow$ be the distances of the dipole from the top and bottom mirrors, respectively, which can be single-layer or multilayer coatings (see Fig. 1). By setting $z = 0$ as the centre of the layer that hosts the dipole and $z = z_0$ as the position of the dipole, one gets

$$d_{\uparrow\downarrow} = \frac{d}{2} \mp z_0, \tag{2.6}$$

where the minus sign corresponds to the upward arrow, while the plus sign corresponds to the downward one. If the complex-amplitude reflectance and transmittance coefficients of the top and bottom mirrors for incidence from inside the dipole-hosting layer are indicated as $r_{\uparrow\downarrow}$ and $t_{\uparrow\downarrow}$, one can verify that the following relationships hold,[4]

$$\rho_{\uparrow\downarrow} = r_{\uparrow\downarrow} \exp\left[-\mathrm{i}kn_0 \left(d \mp 2z_0\right) \cos\theta_0\right], \tag{2.7}$$

$$\tau_{\uparrow\downarrow} = t_{\uparrow\downarrow} \exp\left[-\mathrm{i}kn_0 \left(\frac{d}{2} \mp z_0\right) \cos\theta_0\right], \tag{2.8}$$

$$1 - \rho_\uparrow \rho_\downarrow = 1 - r_\uparrow r_\downarrow \exp\left(-\mathrm{i}2kn_0 d \cos\theta_0\right), \tag{2.9}$$

where k is the amplitude of the free-space wavevector. By using these equations, the outcoupled power corresponding to each orientation of the dipole and polarization state can be written as

$$w_{\uparrow\downarrow} = \frac{n_{\uparrow\downarrow}^2 \cos\theta_{\uparrow\downarrow}}{n_0 \cos\theta_0} F_{\uparrow\downarrow} \left|A_{\uparrow\downarrow} + r_{\downarrow\uparrow} A_{\downarrow\uparrow} \exp\left[-\mathrm{i}kn_0 \left(d \pm 2z_0\right) \cos\theta_0\right]\right|^2, \tag{2.10}$$

where

$$F_{\uparrow\downarrow} = \frac{T_{\uparrow\downarrow}}{\left|1 - r_\uparrow r_\downarrow \exp\left(-\mathrm{i}2kn_0 d \cos\theta_0\right)\right|^2} \tag{2.11}$$

is the Airy function, and

$$T_{\uparrow\downarrow}^s = \frac{n_{\uparrow\downarrow} \cos\theta_{\uparrow\downarrow}}{n_0 \cos\theta_0} \left|t_{\uparrow\downarrow}^s\right|^2, \qquad T_{\uparrow\downarrow}^p = \frac{n_{\uparrow\downarrow} \cos\theta_0}{n_0 \cos\theta_{\uparrow\downarrow}} \left|t_{\uparrow\downarrow}^p\right|^2 \tag{2.12}$$

are the intensity transmittance coefficients of the multilayer mirrors, with superscripts indicating s and p polarizations [36–38]. Equation (2.10) is a compact form that can be applied to any chosen

[4]The used phase convention is that according to which $\exp(-\mathrm{i}kz)$ is a plane wave traveling along the positive direction of the z axis.

orientation—through the $A_{\uparrow\downarrow}$ and $A_{\downarrow\uparrow}$ terms only—and polarization state—through the $A_{\uparrow\downarrow}$, $A_{\downarrow\uparrow}$, $F_{\uparrow\downarrow}$, and $r_{\downarrow\uparrow}$ terms. For a randomly oriented dipole, the s-polarized and p-polarized outcoupled powers are found as superpositions of the elementary-orientation powers, that is [16, 17],

$$w^s_{\uparrow\downarrow} = \frac{2}{3} w^{(h),s}_{\uparrow\downarrow}, \qquad w^p_{\uparrow\downarrow} = \frac{2}{3} w^{(h),p}_{\uparrow\downarrow} + \frac{1}{3} w^{(v),p}_{\uparrow\downarrow}, \tag{2.13}$$

where $w^{(h),s}_{\uparrow\downarrow}$, $w^{(h),p}_{\uparrow\downarrow}$, and $w^{(v),p}_{\uparrow\downarrow}$ are evaluated by means of Eq. (2.10).

2.1 Integration over a numerical aperture

If in the external half space of refractive index $n_{\uparrow\downarrow}$ a detector is placed with detecting surface normal to the z axis and numerical aperture NA, the total detected power is found to be

$$w^{\det}_{\uparrow\downarrow} = w^{s,\det}_{\uparrow\downarrow} + w^{p,\det}_{\uparrow\downarrow}, \tag{2.14}$$

where

$$w^{s,\det}_{\uparrow\downarrow} = 2\pi \int_0^{\theta_{\max}} w^s_{\uparrow\downarrow} \sin\theta_{\uparrow\downarrow} \, \mathrm{d}\theta_{\uparrow\downarrow}, \qquad w^{p,\det}_{\uparrow\downarrow} = 2\pi \int_0^{\theta_{\max}} w^p_{\uparrow\downarrow} \cos^2\theta_{\uparrow\downarrow} \sin\theta_{\uparrow\downarrow} \, \mathrm{d}\theta_{\uparrow\downarrow}, \tag{2.15}$$

and $\theta_{\max} = \sin^{-1}\left(\frac{\mathrm{NA}}{n_{\uparrow\downarrow}}\right)$. In both the integrals, the factor $2\pi \sin\theta_{\uparrow\downarrow}$ comes from the integration over the detection solid angle in polar coordinates, the outcoupled power being revolution-symmetric around the z axis; a further factor $\cos^2\theta_{\uparrow\downarrow}$ is present for the p-polarized component alone because the detector cannot detect components of the electric field that lie along the z axis.

2.2 Example: point source between two ideal mirrors

The very simplest case one can consider is that of a radiating dipole placed inside a cavity consisting of two plane-parallel *ideal* mirrors, that is, mirrors having intensity reflectance and transmittance coefficients, R and T, that ideally depend neither on the angle of incidence nor on polarization. The top and bottom mirrors are assumed to be infinitely thin, non-absorbing (so that $T = 1 - R$), optically equivalent, and with zero-phase response. Moreover, the refractive indices of the internal and external media are assumed for simplicity to be $n_0 = n_{\uparrow\downarrow} = 1$. Any distinction between θ_0 and $\theta_{\uparrow\downarrow}$ becomes pointless in such a case, so that notation can be simplified by setting $\theta_0 = \theta_{\uparrow\downarrow} \equiv \theta$. Under such conditions, one can evaluate the power components of the outcoupled field by using Eqs. (2.1), (2.2) and (2.10), that is

$$w^{(h),s}_{\uparrow\downarrow} = \frac{3}{2} w_0 (1 - R) \frac{1 + R + 2\sqrt{R}\cos\left[k\,(d \pm 2z_0)\cos\theta\right]}{1 + R^2 - 2R\cos\left(2kd\cos\theta\right)}, \tag{2.16}$$

$$w^{(h),p}_{\uparrow\downarrow} = \frac{3}{2} w_0 (1 - R)\cos^2\theta \frac{1 + R + 2\sqrt{R}\cos\left[k\,(d \pm 2z_0)\cos\theta\right]}{1 + R^2 - 2R\cos\left(2kd\cos\theta\right)}, \tag{2.17}$$

$$w^{(v),p}_{\uparrow\downarrow} = 3 w_0 (1 - R)\sin^2\theta \frac{1 + R - 2\sqrt{R}\cos\left[k\,(d \pm 2z_0)\cos\theta\right]}{1 + R^2 - 2R\cos\left(2kd\cos\theta\right)}, \tag{2.18}$$

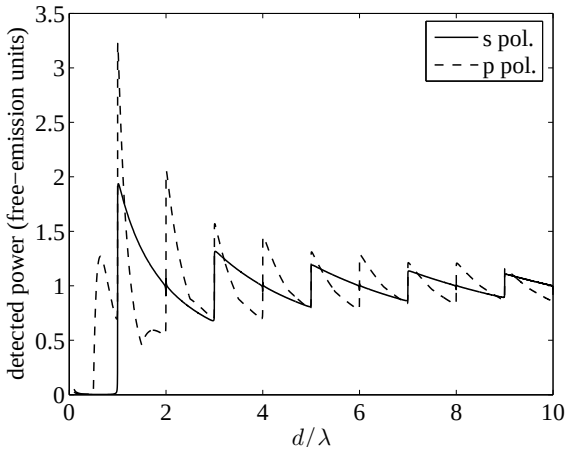

Figure 2. Behavior of the s-polarized and p-polarized components of the detected power coming from a randomly oriented dipole placed at the centre of a cavity ($z_0 = 0$). The power components are detected by an ideally polarization-selective detector of numerical aperture 0.866. The mirror reflectivities are $R = 0.99$ and do not depend on angle of incidence or polarization.

where $w_0 = \frac{1}{8\pi} \approx 0.0398$ is the value of the s-polarized and p-polarized power components radiated by a dipole in free space.[5] In agreement with Eqs. (2.13), the s-polarized and p-polarized components of the outcoupled power radiated from a randomly oriented dipole representing a point source are

$$w^s_{\uparrow\downarrow} = w_0(1-R)\,\frac{1+R+2\sqrt{R}\cos\big[k\,(d\pm 2z_0)\cos\theta\big]}{1+R^2-2R\cos\,(2kd\cos\theta)}, \tag{2.19}$$

$$w^p_{\uparrow\downarrow} = w_0(1-R)\,\frac{1+R+2\sqrt{R}\cos(2\theta)\cos\big[k\,(d\pm 2z_0)\cos\theta\big]}{1+R^2-2R\cos\,(2kd\cos\theta)}, \tag{2.20}$$

where the identity $\cos^2\theta - \sin^2\theta = \cos(2\theta)$ has been used.

As an example, let us assume the dipole to be located at the centre of the cavity, that is, at $z_0 = 0$, and that an ideally polarization-selective detecting system with numerical aperture $\mathrm{NA} = 0.866$, corresponding to $\theta_{\max} = \frac{\pi}{3}$, is used to detect the top half-space outcoupled powers of Eqs. (2.19) and (2.20). Let the mirror reflectivity be $R = 0.99$. The plots of the detected power components—evaluated according to Eqs. (2.15)—*vs.* mirror spacing are shown in Fig. 2. Here, the power components are normalized to the corresponding values that would be found for $R = 0$ (free space), that is, $2\pi(1-\cos\theta_{\max})w_0$ for s polarization and $\frac{2}{3}\pi\,(1-\cos^3\theta_{\max})\,w_0$ for p polarization, while the mirror spacing is normalized to the free-space wavelength, λ. It is worth noting that the two curves in Fig. 2 are suggestive of the inhibition and enhancement properties of a microcavity. As a matter of fact, for mirror spacings d of the same order of λ, one observes emissions larger (enhancement) or lower (inhibition) than in free space.[6] In particular, total inhibition is observed for $d < \lambda$ (s polarization) and $d < \frac{\lambda}{2}$ (p polarization). On the other hand, as the mirror spacing increases with respect to the wavelength, the two curves asymptotically become closer and closer to unity, that is, to the behavior in free space. As a final remark, Fig. 2 is fully consistent with

[5] That is, the $s+p$ radiated power is equal to $\frac{1}{4\pi} \approx 0.0796$. I am omitting units for simplicity.

[6] A deeper analysis of the enhancement and inhibition phenomenon would need to integrate power over all the solid angle, including also modes that can be guided inside the cavity [13].

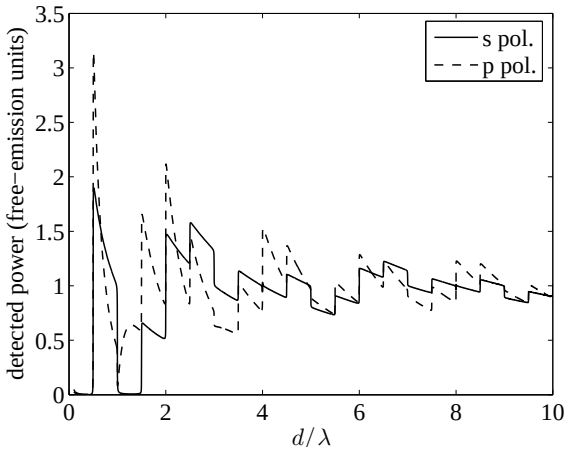

Figure 3. Behavior of the s-polarized and p-polarized components of the detected power (top half space) coming from a randomly oriented dipole placed halfway between the centre of a cavity and its top mirror ($z_0 = \frac{d}{4}$). The power components are detected by an ideally polarization-selective detector of numerical aperture 0.866. The mirror reflectivities are $R = 0.99$ and do not depend on angle of incidence or polarization.

the plots found by Marrocco [40, Fig. 3] by using a different method based on arrays of source images [4, 22].

Figure 3 was obtained with the same settings used for Fig. 2, but this time the dipole was placed at $z_0 = \frac{d}{4}$, that is, halfway between the cavity centre and the top mirror. Here, one can notice a quite different behavior from that shown in Fig. 2. In particular, the higher values of power are found in correspondence of $d = \frac{\lambda}{2}$ instead of $d = \lambda$, while for the latter spacing value the example in Fig. 3 shows total inhibition of emission for both polarizations. Here too, the asymptotic behavior for growing $\frac{d}{\lambda}$ is that of free space.

3 Volume source in a layered medium

The results obtained for the case of a single point source, represented as an elementary randomly-oriented dipole, can be generalized to the case of a volume distribution of sources inside the cavity.

So far, the emitted radiation has been assumed to be fully monochromatic, that is, temporally coherent. Keeping such an approximation also for the following, one has nonetheless to take into account the spatial-coherence properties of the distribution of sources because of the finite extension of the radiating volume. Indeed, two distinct points of the volume radiate with phases that vary randomly in time; therefore, the total power is the result of the interference of two vectors with fluctuating phase difference. As radiated power is detected over time scales that are much longer than the time scale of such variations, the detected signal is a time average of power fluctuations. The degree of mutual phase correlation between the two radiating points indicates how much the two points cooperate in the SpE process, and hence how strongly the radiated fields can mutually interfere [32–34].

In the present paper three cases are discussed: (*a*) the elements of the volume source do not cooperate at all in the SpE process; (*b*) they cooperate with all the other elements (long-range cooperation); (*c*) any source element cooperates with those elements that are located within a certain

range (short-range cooperation). Here, *long*-range and *short*-range refer to cooperation lengths that are long or short, accordingly, with respect to the dimensions of the source. While case *(c)* is thought to represent a more realistic situation for volumes of dimensions of a few wavelengths or more, the other two cases are ideal approximations. Nonetheless, they are mathematically simpler and can help in understanding limiting features of case *(c)*.

3.1 Non-cooperative SpE

If the points of the radiating volume do not cooperate with each other, the elementary powers that are coupled outside the cavity have no mutual phase correlation at all, so that the total power is simply a sum of single components. In mathematical terms, if $\mu(\mathbf{r})$ is the volume-density function of the elementary random dipoles that form the radiating volume, where $\mathbf{r} = (x, y, z)$ is the position vector, the total power is

$$W_{\uparrow\downarrow} = \int \mu(\mathbf{r})\, w_{\uparrow\downarrow}(z)\, \mathrm{d}^3 r, \tag{3.1}$$

which—given an observation angle, $\theta_{\uparrow\downarrow}$—holds for any dipole orientation and polarization state. Clearly, the case of an elementary dipole placed at z_0 is recovered when the volume-density function approaches a three-dimensional Dirac delta distribution centred around z_0, *i.e.*, $\mu(\mathbf{r}) \to \delta(x)\delta(y)\delta(z - z_0)$. For the present case, the x and y positions are irrelevant.

By substituting Eq. (2.10)—with z_0 replaced by z—into Eq. (3.1), one gets

$$\begin{aligned} W_{\uparrow\downarrow} = \frac{n_{\uparrow\downarrow}^2 \cos\theta_{\uparrow\downarrow}}{n_0 \cos\theta_0} F_{\uparrow\downarrow} \Bigg\{ & \left[\left|A_{\uparrow\downarrow}\right|^2 + R_{\downarrow\uparrow} \left|A_{\downarrow\uparrow}\right|^2 \right] N \\ & + 2A_{\uparrow}A_{\downarrow} \mathrm{Re}\left[r_{\downarrow\uparrow} \exp\left(-\mathrm{i}kn_0 d\cos\theta_0\right) \int \mu(\mathbf{r}) \exp\left(\mp \mathrm{i}2kn_0 z\cos\theta_0\right) \mathrm{d}^3 r \right] \Bigg\}, \end{aligned} \tag{3.2}$$

where

$$N = \int \mu(\mathbf{r})\, \mathrm{d}^3 r \tag{3.3}$$

is the number of dipoles in the volume distribution. It is easy to realize that the integral in Eq. (3.2) is the Fourier transform[7] of $\mu(\mathbf{r})$ evaluated at the spatial frequencies

$$(\xi, \eta, \zeta) = \left(0, 0, \pm 2\frac{n_0}{\lambda}\cos\theta_0\right). \tag{3.4}$$

For a few functional forms of $\mu(\mathbf{r})$, this Fourier transform can be evaluated analytically.

[7] The exponential-argument convention is adopted according to which $\int f(x) \exp\left(-\mathrm{i}2\pi\xi x\right) \mathrm{d}x$ is the Fourier transform of $f(x)$ evaluated at the spatial frequency ξ.

3.1.1 Example: cylinder distribution between ideal mirrors

As an example, let us consider a vertical cylinder of diameter D and height $h \leq d$ that is homogeneously filled with N randomly oriented dipoles,[8]

$$\mu(\mathbf{r}) = \begin{cases} \dfrac{4N}{\pi D^2 h}, & \text{if } \sqrt{x^2+y^2} \leq \frac{D}{2} \text{ and } |z-z_0| \leq \frac{h}{2}, \\ 0, & \text{elsewhere.} \end{cases} \tag{3.5}$$

The cylinder must be inside the layer of index n_0, thus z_0 and h should satisfy $|z_0| \leq \frac{d-h}{2}$. The above definition satisfies Eq. (3.3) and allows finding

$$\int \mu(\mathbf{r}) \exp\left(\mp \mathrm{i}2kn_0 z\cos\theta_0\right) \mathrm{d}^3 r = N \operatorname{sinc}\left(2\frac{n_0 h}{\lambda}\cos\theta_0\right) \exp\left(\mp \mathrm{i}2kn_0 z_0 \cos\theta_0\right), \tag{3.6}$$

where the sinc function is defined as $\operatorname{sinc}(u) = \frac{\sin(\pi u)}{\pi u}$.

Assuming, as done for the case of a single elementary dipole (see Sec. 2.2), two *ideal* mirrors of reflectance R, transmittance $1-R$, and unity refractive index for the inner and outer spaces, one obtains

$$W^s_{\uparrow\downarrow} = W_0(1-R)\frac{1+R+2\sqrt{R}\cos\left(kd\cos\theta\right)\operatorname{sinc}\left(2\frac{h}{\lambda}\cos\theta\right)}{1+R^2-2R\cos\left(2kd\cos\theta\right)}, \tag{3.7}$$

$$W^p_{\uparrow\downarrow} = W_0(1-R)\frac{1+R+2\sqrt{R}\cos(2\theta)\cos\left(kd\cos\theta\right)\operatorname{sinc}\left(2\frac{h}{\lambda}\cos\theta\right)}{1+R^2-2R\cos\left(2kd\cos\theta\right)}, \tag{3.8}$$

where the cylinder has been taken to be exactly centred between the mirrors ($z_0 = 0$); $W_0 = \frac{N}{8\pi}$ is the power radiated in free space, *i.e.*, when the mirrors are removed ($R = 0$). It is worth noting that Eqs. (3.7) and (3.8) can be alternatively obtained by integrating, with suitable multiplicative factors, Eqs. (2.19) and (2.20) along z_0 in the interval $-\frac{h}{2} \leq z_0 \leq \frac{h}{2}$. Observe how these powers linearly depend on the number of dipoles and do not depend at all on the cylinder diameter D. This happens because the total power comes from a summation over single powers, no mutual phase difference being involved in the result, and hence Eqs. (3.7) and (3.8) are also the powers radiated by a uniform layer ($D \to \infty$) of thickness h homogeneously filled with point sources. The plots resulting from an integration over a detector of numerical aperture $\mathrm{NA} = 0.866$, corresponding to $\theta_{\max} = \frac{\pi}{3}$, placed in the top half space are shown in Fig. 4 for the example case $h = \frac{\lambda}{4}$.[9] Here, powers are normalized to the corresponding free-space values, that is, $2\pi(1-\cos\theta_{\max})W_0$ for s polarization and $\frac{2}{3}\pi\left(1-\cos^3\theta_{\max}\right)W_0$ for p polarization. As in the examples of Sec. 2.2, large values of $\frac{d}{\lambda}$ frustrate the microcavity effect, while the highest radiation maxima are found in correspondence of $d = \frac{\lambda}{2}$ for both polarization states. Finally, total inhibition is foreseen for $d < \frac{\lambda}{2}$. Another case, corresponding to the same parameters as before, but with the cylinder height filling the whole mirror spacing ($h = d$), is shown in Fig. 5.

[8] Here, a continuous function to represent the actual distribution of dipoles is being used. This is just an approximation, because a more realistic distribution should be discrete, *i.e.*, in the form

$$\mu(\mathbf{r}) = \sum_{m=1}^{N} \delta(x-x_m)\,\delta(y-y_m)\,\delta(z-z_m),$$

where N is the total number of dipoles and (x_m, y_m, z_m) are their positions.

[9] The two polarization components are evaluated by applying Eqs. (2.15) to $W^s_{\uparrow\downarrow}$ and $W^p_{\uparrow\downarrow}$.

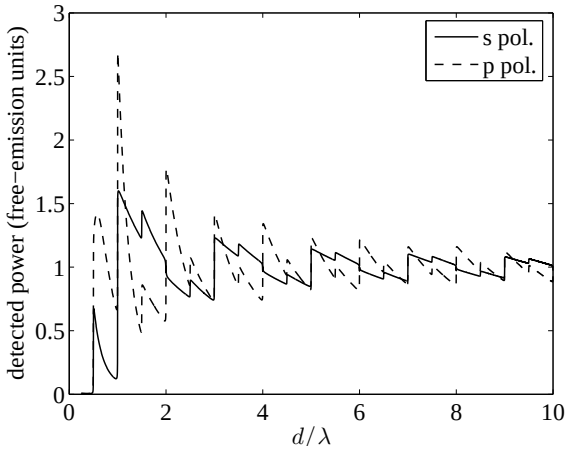

Figure 4. Behavior of the s-polarized and p-polarized components of the detected power (top half space) coming from a vertical cylinder of height $h = \frac{\lambda}{4}$ homogeneously filled with randomly oriented dipoles and centred between the cavity mirrors. No cooperation in the SpE is assumed. The power components are detected by an ideally polarization-selective detector of numerical aperture 0.866. The mirror reflectivities are $R = 0.99$ and do not depend on angle of incidence or polarization.

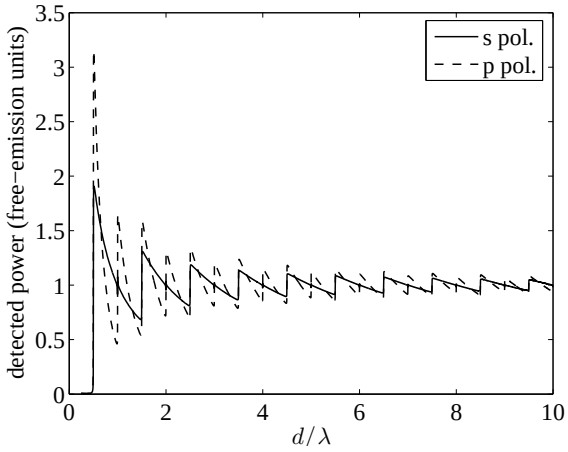

Figure 5. Behavior of the s-polarized and p-polarized components of the detected power (top half space) coming from a vertical cylinder of height $h = d$ homogeneously filled with randomly oriented dipoles and centred between the cavity mirrors. No cooperation in the SpE is assumed. The power components are detected by an ideally polarization-selective detector of numerical aperture 0.866. The mirror reflectivities are $R = 0.99$ and do not depend on angle of incidence or polarization.

3.1.2 Interaction with an optical pump

In Eq. (3.2), $\mu(\mathbf{r})$ is the volume distribution of radiating dipoles. These can represent atomic systems that are excited, *e.g.*, by a laser beam coming from one of the external media (top or bottom). In such a case, one has to take into account that such an optical pump undergoes multireflections at each interface. The problem of finding the pump intensity within the layered medium is addressed in Appendix B. A noteworthy result is that, in case the atomic systems are uniformly distributed and for pump intensities well below saturation, the expression of $\mu(\mathbf{r})$ leads to fully analytical results for the outcoupled powers.

As a matter of fact, if

$$\hat{N}(z) = \begin{cases} \hat{N}_0, & \text{if } |z - z_0| \leq \frac{h}{2}, \\ 0, & \text{elsewhere,} \end{cases} \tag{3.9}$$

with $|z_0| \leq \frac{d-h}{2}$, is the volume density of atomic systems within the layer of index n_0, the resulting distribution $\mu(\mathbf{r})$ of *excited* systems for, *e.g.*, a normally-incident plane-wave optical pump coming from the top medium, is (see Eqs. (B.4) and (B.6) of Appendix B)

$$\mu(\mathbf{r}) = \hat{N}(z)\frac{I_0}{I_{\text{sat}}}\widetilde{F}_{\uparrow}(k_{\text{p}})\left\{1 + R_{\downarrow}(k_{\text{p}}) + 2\sqrt{R_{\downarrow}(k_{\text{p}})}\cos\left[k_{\text{p}}n_0(k_{\text{p}})\,(d+2z) + \phi_{\downarrow}(k_{\text{p}})\right]\right\}, \tag{3.10}$$

with

$$\widetilde{F}_{\uparrow}(k_{\text{p}}) = \frac{\widetilde{T}_{\uparrow}(k_{\text{p}})}{\left|1 - r_{\uparrow}(k_{\text{p}})r_{\downarrow}(k_{\text{p}})\exp\left[-\text{i}2k_{\text{p}}n_0(k_{\text{p}})\,d\right]\right|^2}. \tag{3.11}$$

Here, k_{p} is the free-space wavevector amplitude of the optical pump, I_0 is its intensity in the outer medium, I_{sat} stands for the saturation intensity of the atomic systems, $\phi_{\downarrow}$ is the phase delay—defined in $r_{\downarrow} = \sqrt{R_{\downarrow}}\exp(-\text{i}\phi_{\downarrow})$—introduced on reflection by the bottom layers, and $\widetilde{T}_{\uparrow}$ is the intensity transmittance of the top layers—those that separate the top medium from the layer of index n_0. The tilde over $\widetilde{T}_{\uparrow}$ and $\widetilde{F}_{\uparrow}$ emphasizes that the intensity transmittance coefficient is calculated for incidence from the top medium, that is, reversed with respect to that taken in the formulas for emission. The fact that several parameters—intensity coefficients, amplitude coefficients, and phase delay—are spectrally dispersive and must be taken at the proper pump wavevector has been clearly annotated.

The above form of $\mu(\mathbf{r})$ allows evaluating the net number of atomic systems that participate in the emission and analytically solving Eq. (3.2). The former quantity is

$$\begin{aligned} N = \int \mu(\mathbf{r})\,\mathrm{d}^3r = N_0\frac{I_0}{I_{\text{sat}}}\widetilde{F}_{\uparrow}(k_{\text{p}})\Bigg\{1 + R_{\downarrow}(k_{\text{p}}) \\ + 2\sqrt{R_{\downarrow}(k_{\text{p}})}\cos\left[k_{\text{p}}n_0(k_{\text{p}})\,(d+2z_0) + \phi_{\downarrow}(k_{\text{p}})\right]\text{sinc}\left[\frac{2n_0(k_{\text{p}})h}{\lambda_{\text{p}}}\right]\Bigg\}, \end{aligned} \tag{3.12}$$

where $\lambda_{\text{p}} = \frac{2\pi}{k_{\text{p}}}$ and

$$N_0 = \int \hat{N}(z)\,\mathrm{d}^3r = \hat{N}_0\,\delta^2(0)h \tag{3.13}$$

is the *total* number of atomic systems—either excited or in their ground state. Making explicit the dependence on the emission wavevector, k_e, of the remaining spectrally dispersive quantities and setting $\lambda_\mathrm{e} = \frac{2\pi}{k_\mathrm{e}}$, one obtains

$$\exp\big[-\mathrm{i}k_\mathrm{e}n_0(k_\mathrm{e})\,d\cos\theta_0(k_\mathrm{e})\big]\int\mu(\mathbf{r})\exp\big[\mp\mathrm{i}2k_\mathrm{e}n_0(k_\mathrm{e})\,z\cos\theta_0(k_\mathrm{e})\big]\mathrm{d}^3r \\ = \Gamma_\pm N\exp\big[-\mathrm{i}k_\mathrm{e}n_0(k_\mathrm{e})(d\pm 2z_0)\cos\theta_0(k_\mathrm{e})\big], \quad (3.14)$$

where

$$\Gamma_\pm = \frac{\big[1+R_\downarrow(k_\mathrm{p})\big]\mathrm{sinc}\left[\frac{2n_0(k_\mathrm{e})\,h\cos\theta_0(k_\mathrm{e})}{\lambda_\mathrm{e}}\right] + 2\sqrt{R_\downarrow(k_\mathrm{p})}\,H_\pm}{1+R_\downarrow(k_\mathrm{p})+2\sqrt{R_\downarrow(k_\mathrm{p})}\cos\big[k_\mathrm{p}n_0(k_\mathrm{p})\,(d+2z_0)+\phi_\downarrow(k_\mathrm{p})\big]\,\mathrm{sinc}\left[\frac{2n_0(k_\mathrm{p})h}{\lambda_\mathrm{p}}\right]}, \quad (3.15)$$

$$H_\pm = \frac{\mathrm{i}}{2h\big[k_\mathrm{e}^2n_0^2(k_\mathrm{e})\cos^2\theta_0(k_\mathrm{e}) - k_\mathrm{p}^2n_0^2(k_\mathrm{p})\big]} \\ \times\Big\{k_\mathrm{e}n_0(k_\mathrm{e})\cos\theta_0(k_\mathrm{e})\big[\exp(-\mathrm{i}\Phi)\cos\Psi_\pm - \exp(\mathrm{i}\Phi)\cos\Psi_\mp\big] \\ \pm\mathrm{i}k_\mathrm{p}n_0(k_\mathrm{p})\big[\exp(-\mathrm{i}\Phi)\sin\Psi_\pm - \exp(\mathrm{i}\Phi)\sin\Psi_\mp\big]\Big\}, \quad (3.16)$$

being

$$\Phi = k_\mathrm{e}n_0(k_\mathrm{e})h\cos\theta_0(k_\mathrm{e}), \qquad \Psi_\pm = k_\mathrm{p}n_0(k_\mathrm{p})(d\pm h+2z_0)+\phi_\downarrow(k_\mathrm{p}). \quad (3.17)$$

One can verify that

$$\lim_{h\to 0}H_\pm = \cos\big[k_\mathrm{p}n_0(k_\mathrm{p})(d+2z_0)+\phi_\downarrow(k_\mathrm{p})\big]. \quad (3.18)$$

This means that, for $h\to 0$, $\Gamma_\pm\to 1$ and Eqs. (3.2), (3.12) and (3.14) correctly recover the equation expected for an infinitely thin foil of N pump-excited atomic systems placed at $z=z_0$.

Equations (3.12) and (3.14–3.17) can be substituted into Eq. (3.2) to eventually get fully analytical forms of the outcoupled powers. With obvious meaning of the symbols, the resulting expressions for the s-polarized and p-polarized power components are

$$W_{\uparrow\downarrow}^s = W_0\frac{n_{\uparrow\downarrow}^2(k_\mathrm{e})\cos\theta_{\uparrow\downarrow}(k_\mathrm{e})}{n_0(k_\mathrm{e})\cos\theta_0(k_\mathrm{e})}\,F_{\uparrow\downarrow}^s(k_\mathrm{e})\Big(1+R_{\downarrow\uparrow}^s(k_\mathrm{e}) \\ +2\,\mathrm{Re}\Big\{\Gamma_\pm r_{\downarrow\uparrow}^s(k_\mathrm{e})\exp\big[-\mathrm{i}k_\mathrm{e}n_0(k_\mathrm{e})(d\pm 2z_0)\cos\theta_0(k_\mathrm{e})\big]\Big\}\Big) \quad (3.19)$$

and

$$W_{\uparrow\downarrow}^p = W_0\frac{n_{\uparrow\downarrow}^2(k_\mathrm{e})\cos\theta_{\uparrow\downarrow}(k_\mathrm{e})}{n_0(k_\mathrm{e})\cos\theta_0(k_\mathrm{e})}\,F_{\uparrow\downarrow}^p(k_\mathrm{e})\Big(1+R_{\downarrow\uparrow}^p(k_\mathrm{e}) \\ +2\cos\big[2\theta_0(k_\mathrm{e})\big]\mathrm{Re}\Big\{\Gamma_\pm r_{\downarrow\uparrow}^p(k_\mathrm{e})\exp\big[-\mathrm{i}k_\mathrm{e}n_0(k_\mathrm{e})(d\pm 2z_0)\cos\theta_0(k_\mathrm{e})\big]\Big\}\Big), \quad (3.20)$$

where $W_0=\frac{N}{8\pi}$ is the power radiated in free space by N excited atomic systems.

Similar results can be found also for an optical pump coming from the bottom medium and for non-normal incidence.

3.2 Long-range cooperative SpE

If all the points of the distribution cooperate in the SpE process, the phases of the electric fields radiated by each of them become essential to the evaluation of the total electric field and radiated power. Therefore, one has to generalize Eq. (2.8) by introducing a further phase term that depends also on the transverse coordinates of the dipole position, $\mathbf{r} = (x, y, z)$, that is,

$$\tau_{\uparrow\downarrow} = t_{\uparrow\downarrow} \exp\left[-\mathrm{i}kn_0\left(\frac{d}{2} \mp z\right)\cos\theta_0\right] \exp\big[\mathrm{i}kn_0 \sin\theta_0\,(x\cos\phi + y\sin\phi)\big], \tag{3.21}$$

where ϕ is the azimuthal angle—invariant on refraction—and $z = 0$ has been again assumed to coincide with the centre of the layer the dipoles are embedded in. One can verify that Eqs. (2.7) and (2.9) keep the same form also for the present case.

In presence of long-range cooperation, that is, cooperation over distances that are much longer than the dimensions of the radiating volume, the total electric field that is outcoupled in the far field is the sum of all the elementary electric fields,

$$E_{\uparrow\downarrow} = \int \mu(\mathbf{r})\,\tau_{\uparrow\downarrow} \frac{A_{\uparrow\downarrow} + \rho_{\downarrow\uparrow} A_{\downarrow\uparrow}}{1 - \rho_\uparrow \rho_\downarrow}\,\mathrm{d}^3 r. \tag{3.22}$$

Substituting Eqs. (2.7), (2.9)—with z_0 replaced by z—and (3.21) into Eq. (3.22), one gets

$$E_{\uparrow\downarrow} = \frac{t_{\uparrow\downarrow} \exp\left(-\mathrm{i}\frac{kn_0 d}{2}\cos\theta_0\right)}{1 - r_\uparrow r_\downarrow \exp\left(-\mathrm{i}2kn_0 d\cos\theta_0\right)} \big[A_{\uparrow\downarrow} M_{\uparrow\downarrow} + r_{\downarrow\uparrow} A_{\downarrow\uparrow} M_{\downarrow\uparrow} \exp\left(-\mathrm{i}kn_0 d\cos\theta_0\right)\big], \tag{3.23}$$

where

$$M_{\uparrow\downarrow} = \int \mu(\mathbf{r}) \exp\big[\mathrm{i}kn_0 \sin\theta_0\,(x\cos\phi + y\sin\phi)\big] \exp\left(\pm\mathrm{i}kn_0 z\cos\theta_0\right)\,\mathrm{d}^3 r. \tag{3.24}$$

One can verify that $M_{\uparrow\downarrow}$ is the three-dimensional Fourier transform of $\mu(x, y, z)$ evaluated at the spatial-frequency vector

$$(\xi, \eta, \zeta) = -\frac{n_0}{\lambda}\left(\sin\theta_0\cos\phi, \sin\theta_0\sin\phi, \pm\cos\theta_0\right). \tag{3.25}$$

Note that $M_\uparrow = M_\downarrow$ if $\mu(\mathbf{r})$ is symmetric with respect to z.

Like for the case of a single point source, by taking into account the solid angle transformation on refraction, see Appendix A,[10] the total power that is radiated outside the cavity is

$$W_{\uparrow\downarrow} = \frac{n_{\uparrow\downarrow}^2 \cos\theta_{\uparrow\downarrow}}{n_0\cos\theta_0} F_{\uparrow\downarrow} \big|A_{\uparrow\downarrow} M_{\uparrow\downarrow} + r_{\downarrow\uparrow} A_{\downarrow\uparrow} M_{\downarrow\uparrow} \exp\left(-\mathrm{i}kn_0 d\cos\theta_0\right)\big|^2, \tag{3.26}$$

which should be compared with the corresponding single-dipole expression, see Eq. (2.10). As expected, the latter is recovered when $\mu(\mathbf{r}) = \delta(x - x_0)\,\delta(y - y_0)\,\delta(z - z_0)$.

[10] Since power is detected in the far field, the wave can be considered to be approximately spherical if the dimensions of the volume source are much smaller than the observation distance.

3.2.1 Example: cylinder distribution between ideal mirrors

Let us consider again the cylinder distribution of Eq. (3.5). By exploiting some properties of Fourier transforms, the following result is found

$$M_{\uparrow\downarrow} = N \frac{J_1\left(\pi \frac{n_0 D \sin\theta_0}{\lambda}\right)}{\frac{\pi}{2}\frac{n_0 D \sin\theta_0}{\lambda}} \operatorname{sinc}\left(\frac{n_0 h \cos\theta_0}{\lambda}\right) \exp\left(\pm \mathrm{i} k n_0 z_0 \cos\theta_0\right), \tag{3.27}$$

where $J_1(\cdot)$ is the Bessel function of the first kind and order 1. For ideal mirrors whose reflectivity, R, does not depend on angle of incidence or polarization state, and assuming $n_{\uparrow\downarrow} = n_0 = 1$ and $z_0 = 0$, one obtains

$$W^s_{\uparrow\downarrow} = W_0(1-R)\frac{1 + R + 2\sqrt{R}\cos\left(kd\cos\theta\right)}{1 + R^2 - 2R\cos\left(2kd\cos\theta\right)}, \tag{3.28}$$

$$W^p_{\uparrow\downarrow} = W_0(1-R)\frac{1 + R + 2\sqrt{R}\cos(2\theta)\cos\left(kd\cos\theta\right)}{1 + R^2 - 2R\cos\left(2kd\cos\theta\right)}, \tag{3.29}$$

that is, exactly the same expressions as found for a single random dipole located at $z_0 = 0$, see Eqs. (2.19) and (2.20). This time, however, the free-space radiated power, W_0, which is the same for s and p polarizations, strongly depend on D and on the observation angle,

$$W_0 = N^2 \left[\frac{J_1\left(\pi \frac{D\sin\theta}{\lambda}\right)}{\frac{\pi}{2}\frac{D\sin\theta}{\lambda}}\right]^2 \operatorname{sinc}^2\left(\frac{h\cos\theta}{\lambda}\right). \tag{3.30}$$

Still, along each chosen direction the amplification factor introduced by the cavity is exactly the same for the cooperative cylinder and for a single random dipole at the centre of the cavity,[11] but is slightly different from the amplification factor found for a cylinder in the non-cooperative case, as seen by comparing Eqs. (3.28) and (3.29) with Eqs. (3.7) and (3.8). This means that, at least for a cylinder distribution of random dipoles, the cavity reacts differently depending on the cooperation conditions: in principle, its amplification power is less effective with no cooperation because of the $\operatorname{sinc}\left(2\frac{h}{\lambda}\cos\theta\right)$ factor in Eqs. (3.7) and (3.8), being $\operatorname{sinc}(u) \leq 1$ for any u. Further, note in Eq. (3.30) the dependence of the radiated power on the square power of the number of dipoles, which is a signature of cooperative behavior—this fact holds true both with and without mirrors.

Contrarily to the non-cooperative case, see Sec. 3.1.1, this time the expressions found for the radiated power components depend on the diameter of the cylinder because of the summation of fields instead of powers. For the same reason, the radiated power is strongly influenced by the quantity $\frac{h}{\lambda}$ through the sinc function in Eq. (3.30). For instance, along the normal direction, $\theta = 0$, one has $W_0 = N^2\operatorname{sinc}^2\left(\frac{h}{\lambda}\right)$, which means zero emission for any integer $\frac{h}{\lambda}$, both with and without mirrors, because of destructive interference, no matter what the value of D is.

Choosing, *e.g.*, $d = \lambda$, $h = \frac{\lambda}{4}$ and $D = 2\lambda$, one can plot the angular dependence of the power components radiated by the cylinder both for the non-cooperative and long-range cooperative cases, with and without mirrors. These plots are shown in Fig. 6 and are normalized to N and N^2, respectively. In this figure, one can notice the remarkable difference between the

[11] However, when integration over a numerical aperture is performed, the different angular behaviors of the free-space emissions for the single dipole and cooperative cylinder cases result in distinct responses of the cavity, as shown in the following.

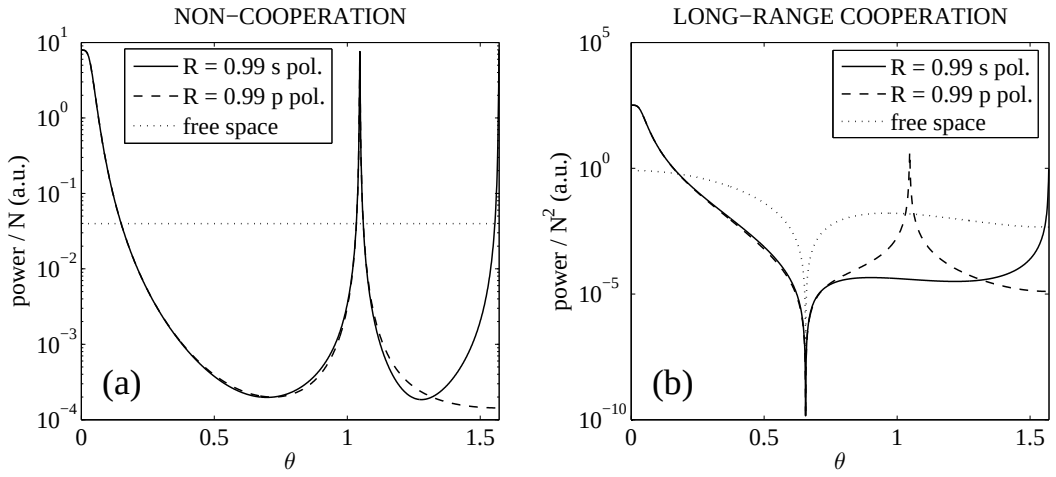

Figure 6. Angular emission from a homogeneous cylinder distribution of random dipoles centred between two mirrors under (a) non-cooperative and (b) long-range cooperative conditions. The mirror spacing is $d = \lambda$. The cylinder diameter and height are $D = 2\lambda$ and $h = \frac{\lambda}{4}$, respectively. The reflectivity of the mirrors, considered as ideal, is $R = 0.99$ and does not depend on incidence angle or polarization state.

non-cooperative (Fig. 6 (a)) and long-range cooperative (Fig. 6 (b)) cases. For the latter, the combination of the amplification effect of the cavity and constructive interference among the dipoles results in much higher outcoupled powers. This is generally true for any integer value of $\frac{d}{\lambda}$, as shown in Fig. 7—which should be compared with Fig. 4 corresponding to the same geometry un-

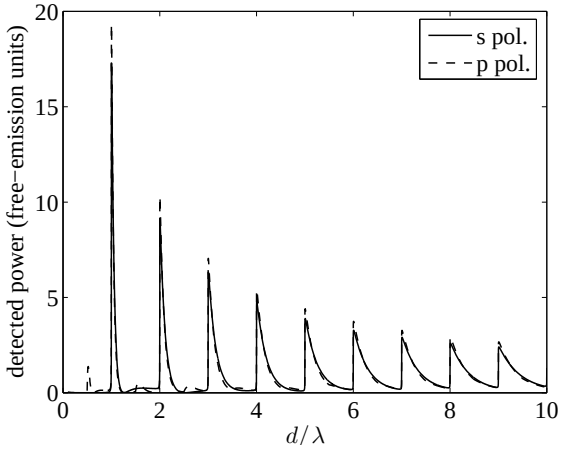

Figure 7. Behavior of the s-polarized and p-polarized components of the detected power (top half space) coming from a vertical cylinder (diameter $D = 2\lambda$ and height $h = \frac{\lambda}{4}$) homogeneously filled with randomly oriented dipoles and centred between two mirrors spaced by d. Long-range cooperation is assumed. The power components are detected by an ideally polarization-selective detector of numerical aperture 0.866. The mirror reflectivities are $R = 0.99$ and do not depend on angle of incidence or polarization.

der non-cooperative conditions—for the same cylinder distribution as above and with long-range cooperation. As usual, in Fig. 7 the power components are also normalized, at each value of d, to the corresponding values that one would obtain by removing the cavity mirrors ($R = 0$).

3.3 Short-range cooperative SpE

Now, let us consider again a volume distribution, $\mu(\mathbf{r})$, of point sources modeled as randomly oriented dipoles. This time, however, short-range cooperation among the single dipoles is assumed: the fields radiated by close enough dipoles will be able to interfere, while for largely spaced dipoles the single powers will sum up with no appreciable interference effect.

3.3.1 Preliminary considerations

Generalizing the method used to describe the effects of spatial coherence in Young's double-slit experiment to a volume distribution [32–34], the outcoupled power can be written as[12]

$$W_{\uparrow\downarrow} = q_{\uparrow\downarrow} \left\langle \int \mu\left(\mathbf{r}\right) E_{\uparrow\downarrow}\left(\mathbf{r}\right) \exp\left[\mathrm{i}\varphi(\mathbf{r},t)\right] \mathrm{d}^3 r \int \mu^*\left(\mathbf{r}'\right) E^*_{\uparrow\downarrow}\left(\mathbf{r}'\right) \exp\left[-\mathrm{i}\varphi(\mathbf{r}',t)\right] \mathrm{d}^3 r' \right\rangle, \quad (3.31)$$

where $q_{\uparrow\downarrow} = \frac{n^3_{\uparrow\downarrow} \cos^2\theta_{\uparrow\downarrow}}{n_0^2 \cos^2\theta_0}$ for s polarization and $q_{\uparrow\downarrow} = \frac{n^3_{\uparrow\downarrow}}{n_0^2}$ for p polarization, and solid-angle transformation on refraction (see Appendix A) has been taken into account.[13] In Eq. (3.31), $\langle \cdot \rangle$ indicates a time average, and the electric fields originated from the space points $\mathbf{r}$ and $\mathbf{r}'$—given by Eqs. (2.1–2.3), (2.7), (2.9), and (3.21)—possess *additional* phase terms, φ, that randomly vary in time, t. For any chosen couple of dipoles, such random phase variations are mutually more and more correlated as the dipoles are closer and closer; on the other hand, if the dipoles are sufficiently far apart, these phase variations are uncorrelated.

Rearranging Eq. (3.31), one finds

$$W_{\uparrow\downarrow} = q_{\uparrow\downarrow} \iint \mu\left(\mathbf{r}\right) \mu^*\left(\mathbf{r}'\right) E_{\uparrow\downarrow}\left(\mathbf{r}\right) E^*_{\uparrow\downarrow}\left(\mathbf{r}'\right) \left\langle \exp\left\{\mathrm{i}\left[\varphi(\mathbf{r},t) - \varphi(\mathbf{r}',t)\right]\right\}\right\rangle \mathrm{d}^3 r\, \mathrm{d}^3 r'. \quad (3.32)$$

Here, $E_{\uparrow\downarrow}\left(\mathbf{r}\right) E^*_{\uparrow\downarrow}\left(\mathbf{r}'\right) \left\langle \exp\left\{\mathrm{i}\left[\varphi(\mathbf{r},t) - \varphi(\mathbf{r}',t)\right]\right\}\right\rangle$ is the so-called *mutual intensity* of light [32–34]. Along the same lines of Refs. 32–34, let us introduce the complex degree of coherence as[14]

$$\gamma\left(\mathbf{r},\mathbf{r}'\right) = \left\langle \exp\left\{\mathrm{i}\left[\varphi(\mathbf{r},t) - \varphi(\mathbf{r}',t)\right]\right\}\right\rangle, \quad (3.33)$$

which satisfies $\gamma\left(\mathbf{r},\mathbf{r}'\right) = \gamma^*\left(\mathbf{r}',\mathbf{r}\right)$ and $0 \leq \left|\gamma\left(\mathbf{r},\mathbf{r}'\right)\right| \leq 1$, as one can verify.[15] One can also prove that $\gamma(\mathbf{r},\mathbf{r}')$ becomes zero when the random phase variations are uncorrelated. Equation (3.33) allows rewriting Eq. (3.32) as

$$W_{\uparrow\downarrow} = q_{\uparrow\downarrow} \iint \gamma\left(\mathbf{r},\mathbf{r}'\right) \mu\left(\mathbf{r}\right) \mu^*\left(\mathbf{r}'\right) E_{\uparrow\downarrow}\left(\mathbf{r}\right) E^*_{\uparrow\downarrow}\left(\mathbf{r}'\right) \mathrm{d}^3 r\, \mathrm{d}^3 r'. \quad (3.34)$$

[12] For the sake of generality, $\mu(\mathbf{r})$ is assumed to be a complex quantity.

[13] For the short-range cooperation case, the far-field power can be considered as produced by the incoherent superposition of spherical waves as long as the cooperation volume associated with the complex degree of coherence—which will be introduced later, see, *e.g.*, Note 17 on page 24—has dimensions that are small in comparison with the observation distance. Therefore, taking into account solid-angle transformation on refraction is still needed.

[14] This definition slightly differs from those used in Refs. 32–34.

[15] Here, $\left|\gamma\left(\mathbf{r},\mathbf{r}'\right)\right| \leq 1$ comes from

$$\left|\gamma\left(\mathbf{r},\mathbf{r}'\right)\right| = \left|\frac{1}{T}\int_t^{t+T} \exp\left\{\mathrm{i}\left[\varphi(\mathbf{r},t') - \varphi(\mathbf{r}',t')\right]\right\} \mathrm{d}t'\right| \leq \frac{1}{T}\int_t^{t+T} \left|\exp\left\{\mathrm{i}\left[\varphi(\mathbf{r},t') - \varphi(\mathbf{r}',t')\right]\right\}\right| \mathrm{d}t' = 1.$$

Because of the first of the above mentioned properties of $\gamma(\mathbf{r},\mathbf{r}')$, $W_{\uparrow\downarrow} = W_{\uparrow\downarrow}^*$ and hence $W_{\uparrow\downarrow}$ is a real quantity.

While the long-range cooperative case can be straightforwardly derived from Eq. (3.34) with the substitution $\gamma(\mathbf{r},\mathbf{r}') = 1$, the derivation of the non-cooperative case needs a deeper analysis. As a matter of fact, for the non-cooperative case one needs to set

$$\gamma(\mathbf{r},\mathbf{r}') = \begin{cases} 1, & \text{if } \mathbf{r} = \mathbf{r}', \\ 0, & \text{otherwise,} \end{cases} \tag{3.35}$$

which satisfies $0 \leq \left|\gamma(\mathbf{r},\mathbf{r}')\right| \leq 1$, as requested. However, replacing Eq. (3.35) into Eq. (3.34), the resulting power seems to be null and therefore different from what foreseen by Eq. (3.1). This apparent contradiction has an explanation: a realistic distribution of point sources is a discrete function rather than continuous. Using the form of $\mu(\mathbf{r})$ shown in Note 8 on page 15, one gets

$$W_{\uparrow\downarrow} = q_{\uparrow\downarrow} \sum_{m=1}^{N} \sum_{m'=1}^{N} \gamma(\mathbf{r}_m,\mathbf{r}_{m'})\, E_{\uparrow\downarrow}(\mathbf{r}_m)\, E_{\uparrow\downarrow}^*(\mathbf{r}_{m'}) \tag{3.36}$$

that, by applying Eq. (3.35), becomes

$$W_{\uparrow\downarrow} = \sum_{m=1}^{N} q_{\uparrow\downarrow} \left|E_{\uparrow\downarrow}(\mathbf{r}_m)\right|^2 = \sum_{m=1}^{N} w_{\uparrow\downarrow}(\mathbf{r}_m)\,. \tag{3.37}$$

The above result is in full agreement with Eq. (3.1).

Therefore, the continuous-distribution approximation can be computationally useful and well working if the dipole spacing is much smaller than the wavelength; however, to deal with limit cases, one has to keep in mind that the underlying real distribution is discrete.

3.3.2 Outcoupled power

Equation (3.34) is the basic equation from which one can find the power outcoupled from inside a cavity by a volume distribution of point sources (random dipoles) under short-range cooperation conditions. As a matter of fact, by taking into account Eqs. (2.1–2.3), (2.7), (2.9), and (3.21), one gets

$$W_{\uparrow\downarrow} = \frac{n_{\uparrow\downarrow}^2 \cos\theta_{\uparrow\downarrow}}{n_0 \cos\theta_0}\, F_{\uparrow\downarrow}\Big\{ A_{\uparrow\downarrow}^2 U_{\uparrow\downarrow} + |r_{\downarrow\uparrow}|^2 A_{\downarrow\uparrow}^2 U_{\downarrow\uparrow} + 2A_{\uparrow}A_{\downarrow}\mathrm{Re}\left[r_{\downarrow\uparrow}\exp\left(-\mathrm{i}kn_0 d\cos\theta_0\right) V_{\downarrow\uparrow}\right]\Big\}, \tag{3.38}$$

where

$$U_{\uparrow\downarrow} = \iint \gamma(\mathbf{r},\mathbf{r}')\,\mu(\mathbf{r})\mu^*(\mathbf{r}') \exp\Big\{\mathrm{i}kn_0 \sin\theta_0 \left[(x-x')\cos\phi + (y-y')\sin\phi\right]\Big\} \times \exp\left[\pm\mathrm{i}kn_0(z-z')\cos\theta_0\right]\, \mathrm{d}^3r\, \mathrm{d}^3r', \tag{3.39}$$

$$V_{\uparrow\downarrow} = \iint \gamma(\mathbf{r},\mathbf{r}')\,\mu(\mathbf{r})\mu^*(\mathbf{r}') \exp\Big\{\mathrm{i}kn_0 \sin\theta_0 \left[(x-x')\cos\phi + (y-y')\sin\phi\right]\Big\} \times \exp\left[\pm\mathrm{i}kn_0(z+z')\cos\theta_0\right]\, \mathrm{d}^3r\, \mathrm{d}^3r'. \tag{3.40}$$

Note that $V_{\uparrow\downarrow}$ differs from $U_{\uparrow\downarrow}$ only for the presence of $(z+z')$, instead of $(z-z')$, inside the integral. Moreover, one can verify that Eqs. (3.38) and (3.26) become the same in the long-range cooperative case, that is, for $\gamma(\mathbf{r},\mathbf{r}')=1$.[16]

Equations (3.38–3.40) deserve a few comments. First, it can be shown that Eq. (3.38) gives a real quantity under the above-mentioned condition $\gamma(\mathbf{r},\mathbf{r}')=\gamma^*(\mathbf{r}',\mathbf{r})$. Second, Eqs. (3.39) and (3.40) are the six-dimensional Fourier transform of $\gamma(\mathbf{r},\mathbf{r}')\,\mu(\mathbf{r})\mu^*(\mathbf{r}')$ evaluated at the spatial-frequency vectors

$$(\xi,\eta,\zeta,\xi',\eta',\zeta') = -\frac{n_0}{\lambda}\left(\sin\theta_0\cos\phi, \sin\theta_0\sin\phi, \pm\cos\theta_0, -\sin\theta_0\cos\phi, -\sin\theta_0\sin\phi, \mp\cos\theta_0\right) \quad (3.41)$$

for $U_{\uparrow\downarrow}$ and

$$(\xi,\eta,\zeta,\xi',\eta',\zeta') = -\frac{n_0}{\lambda}\left(\sin\theta_0\cos\phi, \sin\theta_0\sin\phi, \pm\cos\theta_0, -\sin\theta_0\cos\phi, -\sin\theta_0\sin\phi, \pm\cos\theta_0\right) \quad (3.42)$$

for $V_{\uparrow\downarrow}$. If $\gamma(\mathbf{r},\mathbf{r}')=\gamma_X(x,x')\,\gamma_Y(y,y')\,\gamma_Z(z,z')$, the six-dimensional Fourier transform becomes the product of three two-dimensional transforms. This is the case, for instance, if one chooses to model the complex degree of coherence with a three-dimensional Gaussian (3DG) function, something that also allows obtaining analytical results for suitable volume distributions of dipoles.

3.3.3 Examples with 3DG complex degree of coherence

Let us represent the complex degree of coherence with a 3DG function,

$$\gamma(\mathbf{r},\mathbf{r}') = \exp\left[-\frac{(x-x')^2+(y-y')^2}{L^2}\right]\exp\left[-\frac{(z-z')^2}{L_z^2}\right]. \quad (3.43)$$

Here, L and L_z are two length parameters representative of the cooperation ranges over the Oxy plane and along the z axis, respectively.[17] For symmetry reasons, no distinction has been made along x and y. This kind of complex degree of coherence recalls the characteristics of a Gaussian Schell-model source [34, Ch. 5]; however, it differs from it in the choice of setting $L_z \neq L$.

The so defined complex degree of coherence satisfies all the fundamental properties it should, like $\gamma(\mathbf{r},\mathbf{r}')=1$ for $\mathbf{r}=\mathbf{r}'$ and $\gamma(\mathbf{r},\mathbf{r}')\to 0$ for large $|\mathbf{r}-\mathbf{r}'|$ [32]. The advantage of using it is that, for suitable volume distributions of dipoles, the integrals in Eqs. (3.39) and (3.40) can be evaluated analytically. Two examples are given in the following.

Example 1: ***Uniform distribution of point sources between ideal mirrors***

This case is representative of an active layer placed between two mirrors, *e.g.*, an active layer that electroluminesces. Let us consider a uniform distribution of dipoles in the space interval

[16] Indeed, in such a case, $U_{\uparrow\downarrow}=|M_{\uparrow\downarrow}|^2$ and $V_{\uparrow\downarrow}=M_{\uparrow\downarrow}M_{\downarrow\uparrow}^*$.

[17] Chosen a point source at $\mathbf{r}_0\equiv(x_0,y_0,z_0)$, one can assume its effective "cooperation volume" to be approximately $[x_0-2L,x_0+2L]\times[y_0-2L,y_0+2L]\times[z_0-2L_z,z_0+2L_z]$, as the integral in $\mathbf{r}$ of $\gamma(\mathbf{r},\mathbf{r}_0)$ over this space interval is 98.6% of the same integral over all the space.

$|z - z_0| \leq \frac{h}{2}$, that is,

$$\mu(\mathbf{r}) = \begin{cases} \hat{N}, & \text{if } |z - z_0| \leq \frac{h}{2}, \\ 0, & \text{elsewhere.} \end{cases} \tag{3.44}$$

Here, $\hat{N}$ is the volume density of dipoles, and z_0 and h must satisfy $|z_0| \leq \frac{d-h}{2}$ to confine the distribution within the $-\frac{d}{2} \leq z \leq \frac{d}{2}$ range. Keeping in mind Eq. (3.43), the Fourier transform of $\gamma(\mathbf{r}, \mathbf{r}')\,\mu(\mathbf{r})\mu^*(\mathbf{r}')$ is

$$\mathcal{F}(\xi, \eta, \zeta, \xi', \eta', \zeta') = \hat{N}^2 \mathcal{F}_{XY}(\xi, \eta, \xi', \eta') \mathcal{F}_Z(\zeta, \zeta'), \tag{3.45}$$

with

$$\mathcal{F}_{XY}(\xi, \eta, \xi', \eta') = \pi L^2 \exp\left[-\pi^2 L^2 (\xi^2 + \eta^2)\right] \delta(\xi + \xi')\, \delta(\eta + \eta') \tag{3.46}$$

and

$$\begin{aligned} \mathcal{F}_Z(\zeta, \zeta') = \mathrm{i} L_z \frac{\exp\left[-\mathrm{i}\pi h(\zeta + \zeta')\right] \exp\left[-\pi^2 L_z^2 (\zeta^2 + \zeta'^2)\right]}{4\pi^{1/2}(\zeta + \zeta')} \exp\left[-\mathrm{i}2\pi (\zeta + \zeta') z_0\right] \\ \times \Bigg\{ \exp\left(\pi^2 L_z^2 \zeta^2\right) \left[\operatorname{erf}\left(\frac{h}{L_z} - \mathrm{i}\pi L_z \zeta'\right) - \operatorname{erf}\left(\frac{h}{L_z} + \mathrm{i}\pi L_z \zeta'\right) + 2 \operatorname{erf}\left(\mathrm{i}\pi L_z \zeta'\right) \right] \\ + \exp\left(\pi^2 L_z^2 \zeta'^2\right) \left[\operatorname{erf}\left(\frac{h}{L_z} - \mathrm{i}\pi L_z \zeta\right) - \operatorname{erf}\left(\frac{h}{L_z} + \mathrm{i}\pi L_z \zeta\right) + 2 \operatorname{erf}\left(\mathrm{i}\pi L_z \zeta\right) \right] \\ - \exp\left[\mathrm{i}2\pi h (\zeta + \zeta')\right] \left[\operatorname{erf}\left(\frac{h}{L_z} + \mathrm{i}\pi L_z \zeta\right) + \operatorname{erf}\left(\frac{h}{L_z} + \mathrm{i}\pi L_z \zeta'\right) \right] \\ + \exp\left[\mathrm{i}2\pi h (\zeta + \zeta')\right] \left[\operatorname{erf}\left(\mathrm{i}\pi L_z \zeta\right) + \operatorname{erf}\left(\mathrm{i}\pi L_z \zeta'\right) \right] \Bigg\}. \end{aligned} \tag{3.47}$$

Looking at the form of the spatial-frequency vectors in Eqs. (3.41) and (3.42), one realizes that, to our purposes, Eq. (3.47) can be specialized to the cases $\zeta \to \mp\zeta'$, for which the following simplified forms are obtained

$$\begin{aligned} \mathcal{F}_Z(\zeta, \zeta' \to -\zeta) = L_z^2 \Bigg(\exp\left(-\frac{h^2}{L_z^2}\right) \cos\left(2\pi h\, \zeta\right) - 1 + \pi^{1/2} \exp\left(-\pi^2 L_z^2 \zeta^2\right) \\ \times \left\{ \operatorname{Re}\left[\left(\frac{h}{L_z} + \mathrm{i}\pi L_z \zeta \right) \operatorname{erf}\left(\frac{h}{L_z} + \mathrm{i}\pi L_z \zeta \right) \right] - \mathrm{i}\pi L_z \zeta \operatorname{erf}\left(\mathrm{i}\pi L_z \zeta\right) \right\} \Bigg), \end{aligned} \tag{3.48}$$

$$\begin{aligned} \mathcal{F}_Z(\zeta, \zeta' \to +\zeta) = \frac{L_z \exp\left(-\pi^2 L_z^2 \zeta^2\right)}{2\pi^{1/2} \zeta} \exp\left(-\mathrm{i}4\pi \zeta z_0\right) \\ \times \operatorname{Im}\left\{ \exp\left(\mathrm{i}2\pi h\, \zeta\right) \left[\operatorname{erf}\left(\frac{h}{L_z} + \mathrm{i}\pi L_z \zeta \right) - \operatorname{erf}\left(\mathrm{i}\pi L_z \zeta\right) \right] \right\}. \end{aligned} \tag{3.49}$$

The above Eqs. (3.45–3.49), together with Eqs. (3.41) and (3.42), allow writing

$$U_{\uparrow\downarrow} = \pi\hat{N}^2 L^2 L_z^2\,\delta^2(0)\exp\left(-\pi^2\frac{n_0^2L^2\sin^2\theta_0}{\lambda^2}\right)\left(\exp\left(-\frac{h^2}{L_z^2}\right)\cos\left(2\pi\frac{n_0 h\cos\theta_0}{\lambda}\right)-1\right.$$
$$+\pi^{1/2}\exp\left(-\pi^2\frac{n_0^2L_z^2\cos^2\theta_0}{\lambda^2}\right)\left\{\mathrm{Re}\left[\left(\frac{h}{L_z}\mp\mathrm{i}\pi\frac{n_0L_z\cos\theta_0}{\lambda}\right)\mathrm{erf}\left(\frac{h}{L_z}\mp\mathrm{i}\pi\frac{n_0L_z\cos\theta_0}{\lambda}\right)\right]\right.$$
$$\left.\left.-\ \mathrm{i}\pi\frac{n_0L_z\cos\theta_0}{\lambda}\,\mathrm{erf}\left(\mathrm{i}\pi\frac{n_0L_z\cos\theta_0}{\lambda}\right)\right\}\right), \quad (3.50)$$

$$V_{\uparrow\downarrow} = \mp\frac{\pi^{1/2}\hat{N}^2\lambda L^2 L_z}{2n_0\cos\theta_0}\,\delta^2(0)\exp\left(\pm\mathrm{i}\frac{4\pi n_0 z_0\cos\theta_0}{\lambda}\right)$$
$$\times\exp\left(-\pi^2\frac{n_0^2L^2\sin^2\theta_0}{\lambda^2}\right)\exp\left(-\pi^2\frac{n_0^2L_z^2\cos^2\theta_0}{\lambda^2}\right)$$
$$\times\,\mathrm{Im}\left\{\exp\left(\mp\mathrm{i}2\pi\frac{n_0h\cos\theta_0}{\lambda}\right)\left[\mathrm{erf}\left(\frac{h}{L_z}\mp\mathrm{i}\pi\frac{n_0L_z\cos\theta_0}{\lambda}\right)\pm\mathrm{erf}\left(\mathrm{i}\pi\frac{n_0L_z\cos\theta_0}{\lambda}\right)\right]\right\}. \quad (3.51)$$

These two quantities can be substituted into Eq. (3.38) to evaluate the outcoupled power. Note that the presence of $\delta^2(0)$ in Eqs. (3.50) and (3.51) is simply due to the hypothesized dipole distribution whose extension over Oxy is infinite, therefore one should not worry about it.

Let us consider, once again, ideal mirrors that do not absorb light and whose reflectivity, $R \equiv |r_{\uparrow\downarrow}|^2 = 0.99$, does not depend on angle of incidence or polarization state. The inner and outer refractive index are taken to be $n_0 = n_{\uparrow\downarrow} = 1$. The active layer is assumed to fill all the space between the cavity mirrors, that is, $h = d$ and $z_0 = 0$. As far as the complex degree of coherence is concerned, the cooperation parameters in Eq. (3.43) are chosen to be $L = L_z = \frac{\lambda}{4}$. With these settings, the power that is outcoupled, *e.g.*, in the top half space and there detected by a detector having numerical aperture $\mathrm{NA} = 0.866$ can be evaluated by using Eqs. (3.38) and (2.15). The resulting curves *vs.* mirror spacing are displayed in Fig. 8. Note that the curves in this figure do not differ too much from those found for the non-cooperative case, see Fig. 5. Indeed, as expected, the very same curves as those of Fig. 5 are recovered if one sets $L, L_z \ll \lambda$.

Considering that in an optical microcavity the mode cross section, and hence the transverse correlation between distinct source points, should be larger than in free space [12, 26, 30], the situation remarkably changes if one increases the value of L to, *e.g.*, $L = \lambda$, leaving $L_z = \frac{\lambda}{4}$.[18] The resulting curves are shown in Fig. 9 and demonstrate how the amplifying power of the cavity has increased.

[18]Note, however, that the assumption $L = \lambda$ for any value of d is a naïve one because the mode cross section in a cavity depends on mirror spacing.

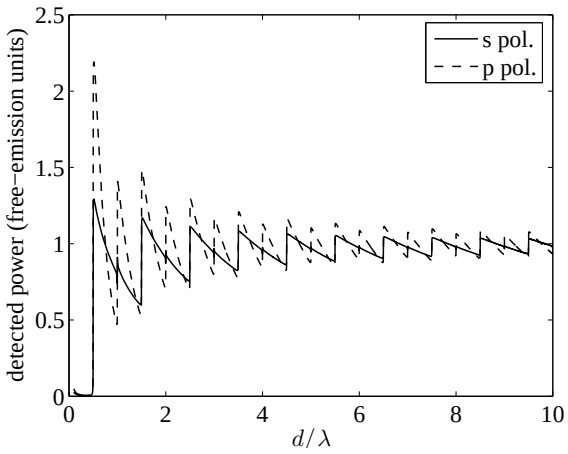

Figure 8. Behavior of the s-polarized and p-polarized components of the detected power (top half space) coming from a uniform distribution of randomly oriented dipoles filling all the space between the two cavity mirrors (distribution height $h = d$ and $z_0 = 0$). Short-range cooperation is assumed, with $L = L_z = \frac{\lambda}{4}$ (see Eq. (3.43)). The power components are detected by an ideally polarization-selective detector of numerical aperture 0.866. The mirror reflectivities are $R = 0.99$ and do not depend on angle of incidence or polarization.

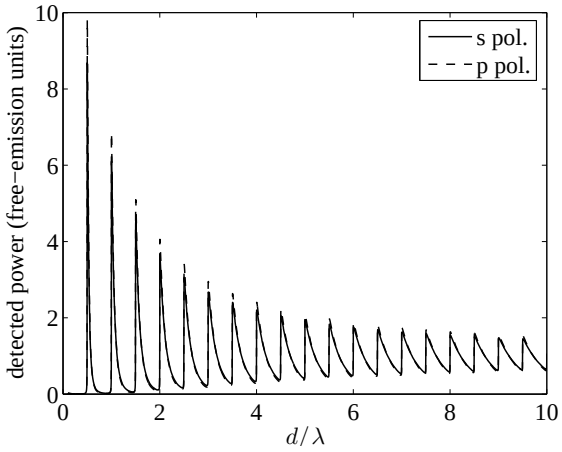

Figure 9. Behavior of the s-polarized and p-polarized components of the detected power (top half space) coming from a uniform distribution of randomly oriented dipoles filling all the space between the two cavity mirrors (distribution height $h = d$ and $z_0 = 0$). Short-range cooperation is assumed, with $L = \lambda$ and $L_z = \frac{\lambda}{4}$ (see Eq. (3.43)). The power components are detected by an ideally polarization-selective detector of numerical aperture 0.866. The mirror reflectivities are $R = 0.99$ and do not depend on angle of incidence or polarization.

Example 2: ***Laser-pumped-like distribution of point sources between ideal mirrors***

In case the active layer is optically pumped by a normally-incident Gaussian laser beam [41], the volume distribution of radiating dipoles can be approximately modeled as[19]

$$\mu(\mathbf{r}) = \begin{cases} \hat{N} \exp\left(-2\,\dfrac{x^2+y^2}{w^2}\right), & \text{if } |z-z_0| \leq \frac{h}{2}, \\ 0, & \text{elsewhere.} \end{cases} \tag{3.52}$$

In the above definition, $\hat{N}$ is again the volume density of random dipoles, z_0 and h must satisfy $|z_0| \leq \frac{d-h}{2}$ to confine the distribution within the $-\frac{d}{2} \leq z \leq \frac{d}{2}$ range, while w is the Gaussian beam waist.

In the present case Eqs. (3.45) and (3.47–3.49) still hold true; on the other hand, Eq. (3.46) has to be replaced with

$$\begin{aligned} \mathcal{F}_{XY}(\xi,\eta,\xi',\eta') = \frac{\pi^2 L^2 w^4}{4\left(L^2+w^2\right)} \exp\left\{-\frac{\pi^2 w^2}{4\left(L^2+w^2\right)}\left[w^2\left(\xi+\xi'\right)^2 + 2L^2\left(\xi^2+\xi'^2\right)\right]\right\} \\ \times \exp\left\{-\frac{\pi^2 w^2}{4\left(L^2+w^2\right)}\left[w^2\left(\eta+\eta'\right)^2 + 2L^2\left(\eta^2+\eta'^2\right)\right]\right\}. \end{aligned} \tag{3.53}$$

This equation simplifies to

$$\begin{aligned} \mathcal{F}_{XY}(\xi,\eta,\xi',\eta') = \frac{\pi^2 L^2 w^2}{4} \exp\left\{-\frac{\pi^2}{4}\left[w^2\left(\xi+\xi'\right)^2 + 2L^2\left(\xi^2+\xi'^2\right)\right]\right\} \\ \times \exp\left\{-\frac{\pi^2}{4}\left[w^2\left(\eta+\eta'\right)^2 + 2L^2\left(\eta^2+\eta'^2\right)\right]\right\} \end{aligned} \tag{3.54}$$

in the very likely case $w^2 \gg L^2$. By applying the substitutions shown in Eqs. (3.41) and (3.42) to Eq. (3.54), one finally finds

$$\begin{aligned} U_{\uparrow\downarrow} = \frac{\pi^2 \hat{N}^2 L^2 L_z^2 w^2}{4} \exp\left(-\pi^2 \frac{n_0^2 L^2 \sin^2\theta_0}{\lambda^2}\right) \left(\exp\left(-\frac{h^2}{L_z^2}\right) \cos\left(2\pi \frac{n_0 h \cos\theta_0}{\lambda}\right) - 1 \right. \\ + \pi^{1/2} \exp\left(-\pi^2 \frac{n_0^2 L_z^2 \cos^2\theta_0}{\lambda^2}\right) \left\{ \mathrm{Re}\left[\left(\frac{h}{L_z} \mp \mathrm{i}\pi \frac{n_0 L_z \cos\theta_0}{\lambda}\right) \mathrm{erf}\left(\frac{h}{L_z} \mp \mathrm{i}\pi \frac{n_0 L_z \cos\theta_0}{\lambda}\right)\right] \right. \\ \left. \left. - \mathrm{i}\pi \frac{n_0 L_z \cos\theta_0}{\lambda} \mathrm{erf}\left(\mathrm{i}\pi \frac{n_0 L_z \cos\theta_0}{\lambda}\right) \right\} \right), \end{aligned} \tag{3.55}$$

$$\begin{aligned} V_{\uparrow\downarrow} = \mp \frac{\pi^{3/2} \hat{N}^2 \lambda L^2 L_z w^2}{8 n_0 \cos\theta_0} \exp\left(\pm \mathrm{i} \frac{4\pi n_0 z_0 \cos\theta_0}{\lambda}\right) \\ \times \exp\left(-\pi^2 \frac{n_0^2 L^2 \sin^2\theta_0}{\lambda^2}\right) \exp\left(-\pi^2 \frac{n_0^2 L_z^2 \cos^2\theta_0}{\lambda^2}\right) \\ \times \mathrm{Im}\left\{ \exp\left(\mp \mathrm{i}\, 2\pi \frac{n_0 h \cos\theta_0}{\lambda}\right) \left[\mathrm{erf}\left(\frac{h}{L_z} \mp \mathrm{i}\pi \frac{n_0 L_z \cos\theta_0}{\lambda}\right) \pm \mathrm{erf}\left(\mathrm{i}\pi \frac{n_0 L_z \cos\theta_0}{\lambda}\right)\right] \right\}. \end{aligned} \tag{3.56}$$

[19] The approximation consists in disregarding the variation of w and $\hat{N}$ along z [41].

Equations (3.55) and (3.56) are exactly the same as Eqs. (3.50) and (3.51) provided the substitution $\delta^2(0) \rightarrow \frac{\pi w^2}{4}$ is performed in the first factor of the latter ones. This finding means that, under the likely condition $w^2 \gg L^2$ and the approximation of constant w and $\hat{N}$ along z within the source volume, the angular dependence of the radiated power is exactly the same for uniform and Gaussian cross sections over Oxy of the volume distribution of radiating dipoles.

4 Electroluminescence from an Alq_3-based OLED

Here, the theory developed in the previous Sections is applied to the real case of an OLED, in which the active layer is Alq_3 [42, 43]. The device is designed with two configurations, see Fig. 10, one of which includes an ultra-thin layer of lithium fluoride (LiF) to form an Al/LiF cathode, a

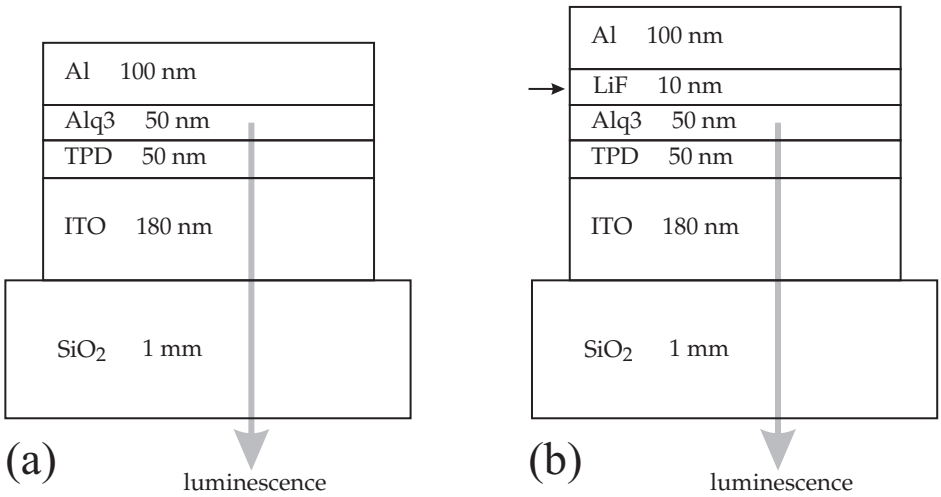

Figure 10. Multilayer OLEDs that have been considered in the simulations: (a) 4-layer OLED; (b) 5-layer OLED obtained with the interposition of an ultra-thin LiF layer between the Al cathode and the Alq_3 active layer (Al/LiF cathode).

configuration that significantly reduces the threshold voltage in Alq_3-based OLED [43, 44]. Our purpose is to evaluate whether the addition of the ultra-thin LiF layer also improves the active optical properties of the device or not. The considered emission wavelength is $\lambda = 530$ nm [43]. The complex refractive indices of the materials that form the device are listed in Tab. 1.

Material	Refractive index
Al	$0.867 - \mathrm{i}\,6.42$ [45]
Alq_3	1.70 [46]
ITO	$2.00 - \mathrm{i}\,0.0085$ [47]
LiF	1.393 [48]
SiO_2	1.547 [45]
TPD	1.85 [46]

Table 1. Complex refractive indices at $\lambda = 530$ nm of the materials considered for the Alq_3-based OLED structures shown in Fig. 10.

The reflectivity and transmittivity coefficients of the layers placed above and below the Alq_3 active layer can be evaluated at all the angles of incidence by using the common method of characteristic matrices [36–38]. The resulting curves are plotted in Fig. 11 *vs.* the incidence angle (evaluated in air). In this figure, one can see that the values of $R_\uparrow \equiv |r_\uparrow|^2$ evaluated without the

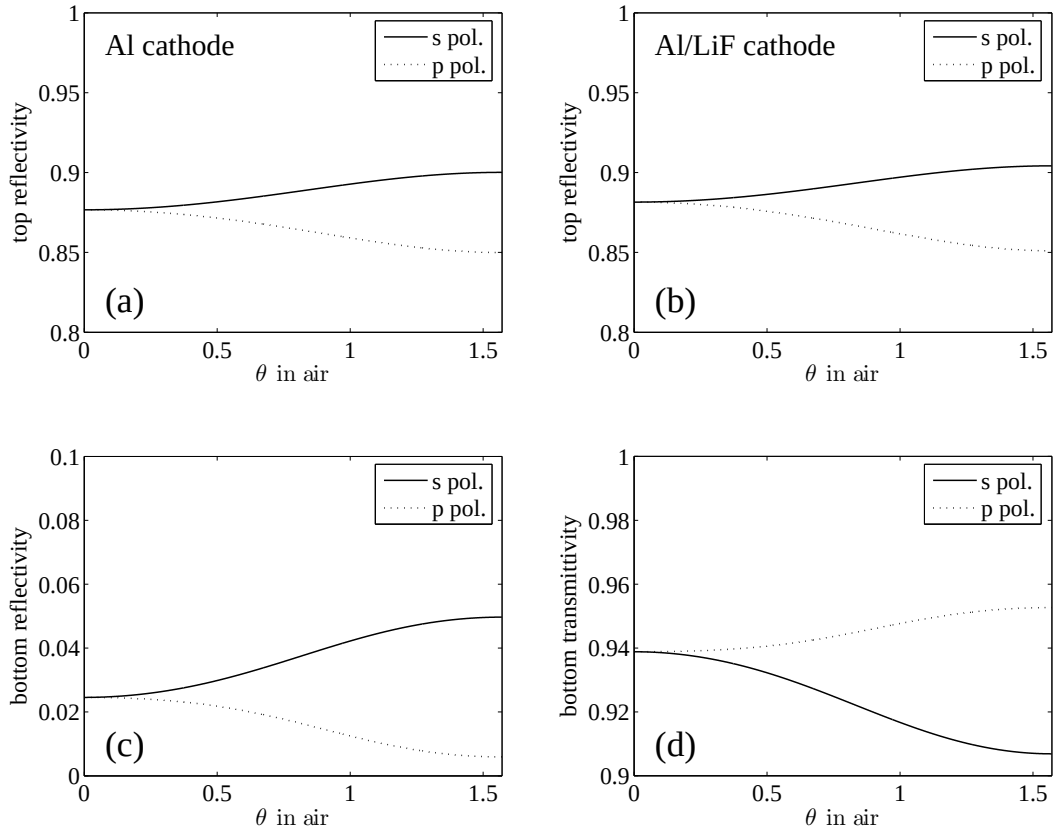

Figure 11. Reflectivity and transmittivity curves at $\lambda = 530$ nm of the layers above and below the Alq_3 layer, for incidence from inside it, as functions of the incidence angle. The equivalent incidence angle in air, found by means of Snell's law, is shown in abscissas. The considered cases are: (a) reflectivity of the top Al cathode of Fig. 10 (a); (b) reflectivity of the top Al/LiF cathode of Fig. 10 (b); (c) reflectivity of the bottom layers of Fig. 10; (d) transmittivity of the bottom layers of Fig. 10—in these two latter cases SiO_2 is the exit medium.

LiF interlayer (Fig. 11 (a)) do not differ too much from those evaluated after having inserted the LiF interlayer (Fig. 11 (b)). The low reflectivity of the bottom layers (Fig. 11 (c)) demonstrates that the device is not comparable with a full cavity; rather, it has to be regarded as a half cavity, whose mirror is formed by the layers placed above the Alq_3 layer—either Al or Al/LiF. As far as the phase delay on reflection from the cathode is concerned, one can compare the results obtained for the Al and Al/LiF cathodes, which are shown in Fig. 12. Here, one can notice that, in the paraxial angular range, the introduction of the ultra-thin LiF layer decreases the phase delay by ~ 0.39 rad, corresponding to an optical path variation of about 33 nm, *i.e.*, $\sim \frac{\lambda}{16}$.

As we are considering electroluminescence escaping into air, the maximum angle inside the Alq_3

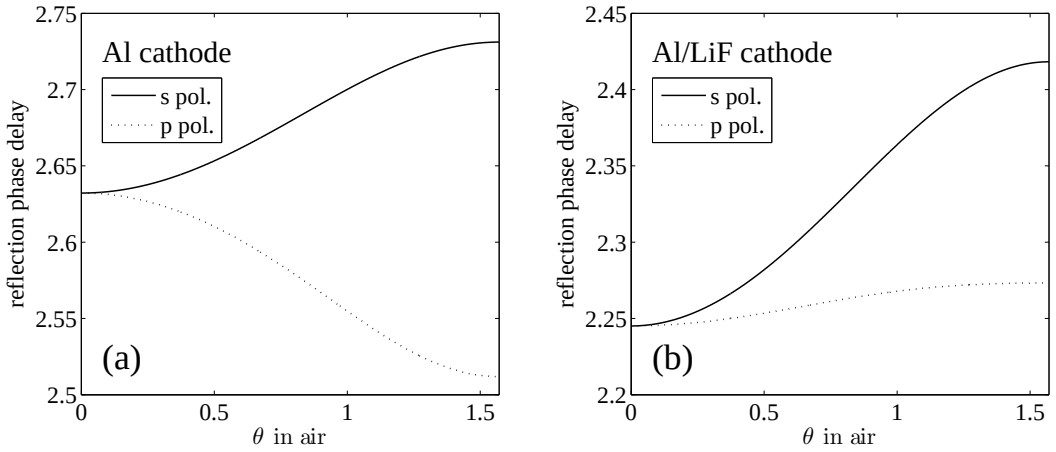

Figure 12. Phase delays on reflection from the cathode at $\lambda = 530$ nm for incidence from inside the Alq_3 layer, as functions of the incidence angle. The equivalent incidence angle in air, found by means of Snell's law, is shown in abscissas. The considered cases are: (a) Al cathode; (b) Al/LiF cathode.

layer along which the radiated power can be outcoupled is $\max\theta_{\mathrm{Alq_3}} = \sin^{-1}\left(\frac{1}{1.70}\right) \approx 0.629$ rad ≈ 36.0 deg, corresponding to $\theta = \frac{\pi}{2}$ in air. Larger angles give rise to evanescent waves in the outer material and possibly to guided modes, which are not of interest in the present work.

4.1 Application of the non-cooperative model

To evaluate the power outcoupled in the bottom half space, let us first consider the non-cooperative model of Sec. 3.1. According to it, the power radiated into the SiO_2 substrate can be estimated by means of Eq. (3.2). Therefore, by adapting Eq. (3.2) to the present case, the power that is radiated into the substrate is

$$W_{\downarrow} = \hat{N} d \, \frac{n_{\mathrm{SiO_2}}^2 \cos\theta_{\mathrm{SiO_2}}}{n_{\mathrm{Alq_3}} \cos\theta_{\mathrm{Alq_3}}} \, F_{\downarrow} \Bigg\{ \left|A_{\downarrow}\right|^2 + R_{\uparrow} \left|A_{\uparrow}\right|^2 + 2A_{\uparrow}A_{\downarrow} \, \mathrm{sinc}\left(\frac{2n_{\mathrm{Alq_3}} d \cos\theta_{\mathrm{Alq_3}}}{\lambda}\right) \mathrm{Re}\left[r_{\uparrow} \exp\left(-\mathrm{i}kn_{\mathrm{Alq_3}} d \cos\theta_{\mathrm{Alq_3}}\right)\right] \Bigg\}, \quad (4.1)$$

with d corresponding to the thickness of the Alq_3 layer, and with obvious meaning of the refractive-index and angle subscripts. To derive Eq. (4.1), a homogeneous distribution of radiating centres of volume density $\hat{N}$ in the Alq_3 layer has been taken—this assumption is a consequence of thinking that the Alq_3 layer is uniformly pumped by the electric field applied to the OLED. An unessential factor $\delta^2(0)$, coming from the infinite extension of the Alq_3 layer over the Oxy plane, has been omitted in Eq. (4.1). The term $F_{\downarrow}$, see Eq. (2.11), is

$$F_{\downarrow} = \frac{T_{\downarrow}}{\left|1 - r_{\uparrow} r_{\downarrow} \exp\left(-\mathrm{i}2kn_{\mathrm{Alq_3}} d \cos\theta_{\mathrm{Alq_3}}\right)\right|^2}. \quad (4.2)$$

Finally, $r_{\uparrow}$ and $R_{\uparrow} \equiv |r_{\uparrow}|^2$ are the complex-amplitude and intensity reflection coefficients of the cathode, respectively, while $T_{\downarrow}$ and $r_{\downarrow}$ are the intensity transmission coefficient and complex-amplitude reflection coefficient of the layers placed between the Alq_3 layer and the SiO_2 substrate,

respectively, with exit medium set as SiO_2 (see Fig. 11). Obviously, Eqs. (4.1) and (4.2) have to be specialized to the two polarizations states, s and p. By doing so, one gets the following equations for the power components that are radiated into the substrate

$$W_{\downarrow}^{s} = \frac{\hat{N}d}{8\pi} \frac{n_{\mathrm{SiO_2}}^2 \cos\theta_{\mathrm{SiO_2}}}{n_{\mathrm{Alq_3}} \cos\theta_{\mathrm{Alq_3}}} F_{\downarrow}^{s} \Bigg\{ 1 + R_{\uparrow}^{s} + 2\,\mathrm{sinc}\left(\frac{2n_{\mathrm{Alq_3}} d \cos\theta_{\mathrm{Alq_3}}}{\lambda} \right) \mathrm{Re}\big[r_{\uparrow}^{s} \exp\left(-\mathrm{i}kn_{\mathrm{Alq_3}} d \cos\theta_{\mathrm{Alq_3}}\right) \big] \Bigg\}, \quad (4.3)$$

$$W_{\downarrow}^{p} = \frac{\hat{N}d}{8\pi} \frac{n_{\mathrm{SiO_2}}^2 \cos\theta_{\mathrm{SiO_2}}}{n_{\mathrm{Alq_3}} \cos\theta_{\mathrm{Alq_3}}} F_{\downarrow}^{p} \Bigg\{ 1 + R_{\uparrow}^{p} + 2\cos\left(2\theta_{\mathrm{Alq_3}}\right)\,\mathrm{sinc}\left(\frac{2n_{\mathrm{Alq_3}} d \cos\theta_{\mathrm{Alq_3}}}{\lambda} \right) \mathrm{Re}\big[r_{\uparrow}^{p} \exp\left(-\mathrm{i}kn_{\mathrm{Alq_3}} d \cos\theta_{\mathrm{Alq_3}}\right) \big] \Bigg\}. \quad (4.4)$$

Assuming the SiO_2 substrate to be optically thick,[20] the power outcoupled in the bottom half space (air) is then obtained by summing the *powers* that are multireflected within the substrate and then transmitted through its bottom face [38]. Moreover, one has to apply a transformation of solid angle for the passage from SiO_2 to air, as explained in Appendix A. The resulting power components that can be detected in the bottom half space—air is assumed to have unitary refractive index—are therefore[21]

$$\widetilde{W}_{\downarrow} = \frac{\cos\theta}{n_{\mathrm{SiO_2}}^2 \cos\theta_{\mathrm{SiO_2}}} \frac{T_0}{1 - R_0 R_{\mathrm{sup}}} W_{\downarrow}, \quad (4.5)$$

which can be applied to any of Eqs. (4.3) and (4.4) by selecting the proper polarization. In Eq. (4.5), θ is the propagation angle in air, R_0 and T_0 are the reflection and transmission intensity coefficients of the SiO_2-air interface, respectively, and R_{sup} is the reflection intensity coefficient of *all* the layers over the substrate. The three latter coefficients are evaluated for incidence from inside the SiO_2 substrate, and depend on angle of incidence and polarization.

The plots shown in Fig. 13 were obtained with Eqs. (4.3–4.5). In this figure, powers are normalized to a common arbitrary factor. The figure compares the power components obtained with (a) the simple Al cathode and (b) the Al/LiF cathode. It is evident how the inclusion of the ultrathin LiF layer improves the extraction efficiency of the device. With the integration of *total* powers over the bottom half solid angle, $2\pi \int_0^{\pi/2} \left(\widetilde{W}_{\downarrow}^{s} + \widetilde{W}_{\downarrow}^{p} \right) \sin\theta \, \mathrm{d}\theta$, one finds that the overall extraction efficiency increases by $\sim 28\%$. Along the normal direction, $\theta = 0$, the efficiency increase is even more evident, equal to $\sim 42\%$. Such an improvement can be ascribed to the phase-delay change shown in Fig. 12, which very likely makes the phases of the internal multireflections better aligned and hence able to give rise to larger constructive interference. The very small reflectivity increase of the cathode after insertion of the LiF layer—see Figs. 11 (a) and (b)—is thought to give a rather negligible contribution to this phenomenon.

[20] That is, thicker than the coherence length of radiation.

[21] The second factor, which describes the effect of multireflections within the substrate, comes from [38]

$$T_0 \sum_{m=0}^{\infty} \left(R_0 R_{\mathrm{sup}} \right)^m = \frac{T_0}{1 - R_0 R_{\mathrm{sup}}}.$$

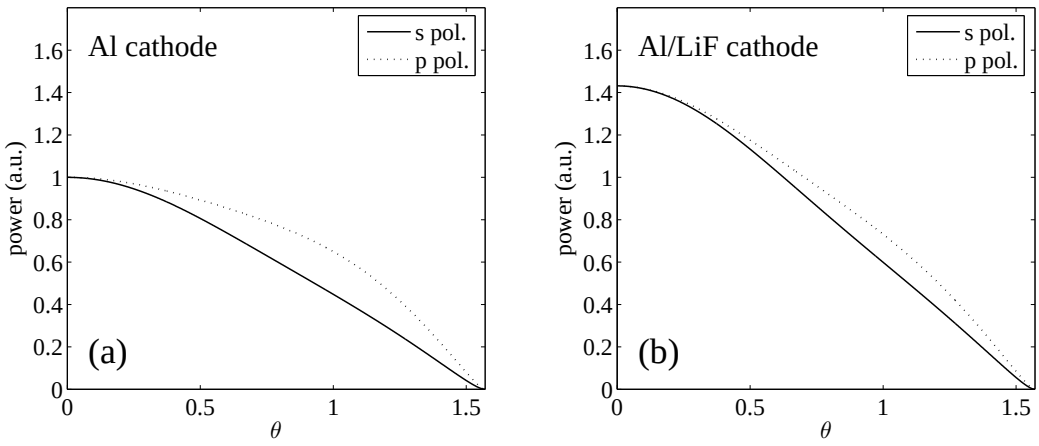

Figure 13. Power components radiated in the bottom half space at $\lambda = 530$ nm by the two OLED configurations shown in Fig. 10. The two cases refer to (a) the simple Al cathode and (b) the Al/LiF cathode. The elements of the active Alq_3 layer are assumed not to cooperate in SpE.

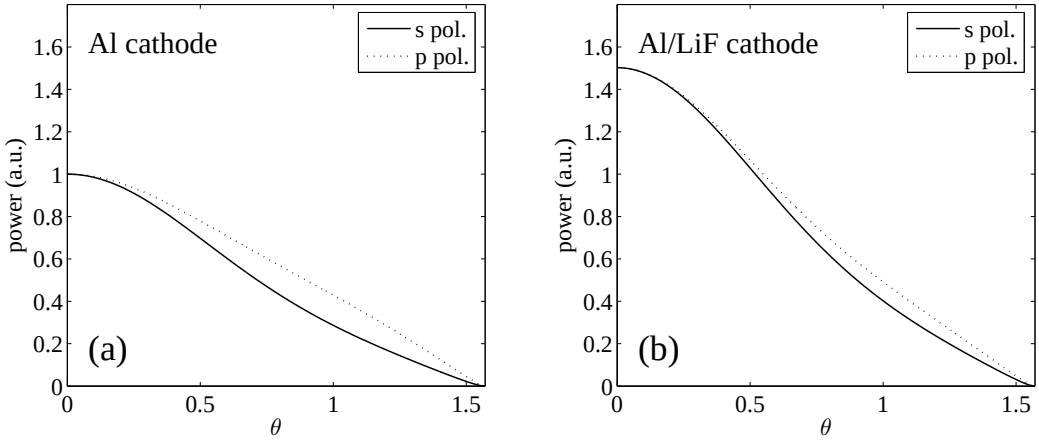

Figure 14. Power components radiated in the bottom half space at $\lambda = 530$ nm by the two OLED configurations shown in Fig. 10. The two cases refer to (a) the simple Al cathode and (b) the Al/LiF cathode. The elements of the active Alq_3 layer are assumed to short-range cooperate to SpE, with the cooperation parameter L set as equal to $\frac{\lambda}{4}$.

4.2 Application of the short-range cooperative model

In the literature, the method of power summation over the active layer thickness—used in Sec. 4.1—is very common to find the power outcoupled from layered devices, such as microcavities. Such an approach relies on the assumption that nearby points of the volume source never cooperate on SpE, no matter how close they are. However, the elements of any extended source must possess a non-zero degree of cooperation (spatial coherence), otherwise the source would not radiate at all [32]. Therefore, it is worth checking what results one would find by applying a better fitting model, like the one developed in Sec. 3.3, and compare them with the plots of Fig. 13.

Assuming for simplicity a 3DG complex degree of coherence, see Eq. (3.43), and the same dipole distribution as in Sec. 4.1, the power $W_\downarrow$ radiated into the SiO_2 substrate can be evaluated by means of Eq. (3.38), which gives

$$W_\downarrow^s = \frac{n_{\mathrm{SiO_2}}^2 \cos\theta_{\mathrm{SiO_2}}}{8\pi n_{\mathrm{Alq_3}} \cos\theta_{\mathrm{Alq_3}}} F_\downarrow^s \Big\{ U_\downarrow + R_\uparrow^s U_\uparrow + 2\,\mathrm{Re}\left[r_\uparrow^s \exp\left(-\mathrm{i}kn_{\mathrm{Alq_3}} d\cos\theta_{\mathrm{Alq_3}}\right) V_\uparrow \right] \Big\}, \tag{4.6}$$

$$\begin{aligned} W_\downarrow^p = {} & \frac{n_{\mathrm{SiO_2}}^2 \cos\theta_{\mathrm{SiO_2}}}{8\pi n_{\mathrm{Alq_3}} \cos\theta_{\mathrm{Alq_3}}} F_\downarrow^p \\ & \times \Big\{ U_\downarrow + R_\uparrow^p U_\uparrow + 2\cos\left(2\theta_{\mathrm{Alq_3}}\right) \mathrm{Re}\left[r_\uparrow^p \exp\left(-\mathrm{i}kn_{\mathrm{Alq_3}} d\cos\theta_{\mathrm{Alq_3}}\right) V_\uparrow \right] \Big\}, \end{aligned} \tag{4.7}$$

where (see Eqs. (3.50) and (3.51))

$$\begin{aligned} U_{\uparrow\downarrow} = {} & \pi \hat{N}^2 L^4 \exp\left(-\pi^2 \frac{n_{\mathrm{Alq_3}}^2 L^2 \sin^2\theta_{\mathrm{Alq_3}}}{\lambda^2} \right) \\ & \times \left(\exp\left(-\frac{d^2}{L^2} \right) \cos\left(2\pi \frac{n_{\mathrm{Alq_3}} d\cos\theta_{\mathrm{Alq_3}}}{\lambda} \right) - 1 + \pi^{1/2} \exp\left(-\pi^2 \frac{n_{\mathrm{Alq_3}}^2 L^2 \cos^2\theta_{\mathrm{Alq_3}}}{\lambda^2} \right) \right. \\ & \times \left\{ \mathrm{Re}\left[\left(\frac{d}{L} \mp \mathrm{i}\pi \frac{n_{\mathrm{Alq_3}} L\cos\theta_{\mathrm{Alq_3}}}{\lambda} \right) \mathrm{erf}\left(\frac{d}{L} \mp \mathrm{i}\pi \frac{n_{\mathrm{Alq_3}} L\cos\theta_{\mathrm{Alq_3}}}{\lambda} \right) \right] \right. \\ & \left. \left. - \mathrm{i}\pi \frac{n_{\mathrm{Alq_3}} L\cos\theta_{\mathrm{Alq_3}}}{\lambda} \mathrm{erf}\left(\mathrm{i}\pi \frac{n_{\mathrm{Alq_3}} L\cos\theta_{\mathrm{Alq_3}}}{\lambda} \right) \right\} \right), \end{aligned} \tag{4.8}$$

$$\begin{aligned} V_\uparrow = {} & -\frac{\pi^{1/2} \hat{N}^2 \lambda L^3}{2 n_{\mathrm{Alq_3}} \cos\theta_{\mathrm{Alq_3}}} \exp\left(-\pi^2 \frac{n_{\mathrm{Alq_3}}^2 L^2}{\lambda^2} \right) \mathrm{Im}\left\{ \exp\left(-\mathrm{i}2\pi \frac{n_{\mathrm{Alq_3}} d\cos\theta_{\mathrm{Alq_3}}}{\lambda} \right) \right. \\ & \left. \times \left[\mathrm{erf}\left(\frac{d}{L} - \mathrm{i}\pi \frac{n_{\mathrm{Alq_3}} L\cos\theta_{\mathrm{Alq_3}}}{\lambda} \right) + \mathrm{erf}\left(\mathrm{i}\pi \frac{n_{\mathrm{Alq_3}} L\cos\theta_{\mathrm{Alq_3}}}{\lambda} \right) \right] \right\}. \end{aligned} \tag{4.9}$$

Here too, as in Sec. 4.1, the common unessential factor $\delta^2(0)$ has been omitted, and $L_z = L$ has been assumed. Assuming $L = \frac{\lambda}{4}$ and using again the substrate correction shown in Eq. (4.5), one gets the power curves that are shown in Fig. 14. In this figure, too, powers are normalized to an arbitrary common factor. A comparison between Fig. 13 and Fig. 14 demonstrates that the introduction of short-range cooperation slightly modifies the power dependence on the observation

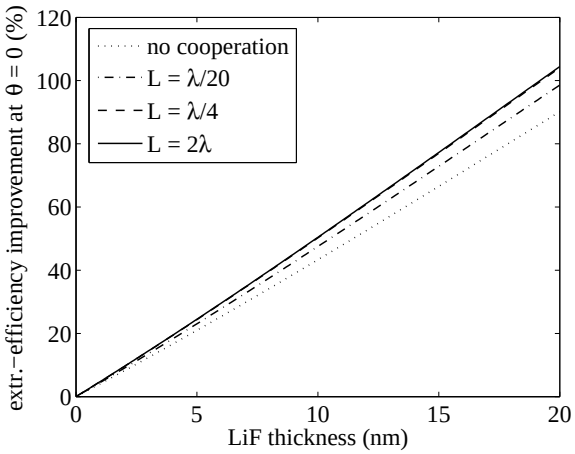

Figure 15. Improvement of extraction efficiency of the Alq_3-based OLED along the normal direction ($\theta = 0$) as a function of LiF thickness. Observe that the $L = \lambda/4$ and $L = 2\lambda$ curves are almost indistinguishable.

angle θ;[22] nonetheless, the extraction efficiency improvement due to the Al/LiF cathode is clearly visible in Fig. 14, as well. In this case, the efficiency improvement found with an integration over the half solid angle in the bottom half space is of $\sim 33\%$, while that along the normal direction is of $\sim 50\%$—both of them being better than in the non-cooperative case. The extraction efficiency improvement along the normal direction, $\theta = 0$, is plotted in Fig. 15 as a function of the the ultra-thin LiF layer thickness for some values of the parameter L, including the case of no cooperation at all ($L \ll \lambda$). The trends show that this efficiency improves linearly for growing values of the LiF layer thickness. One can see how quite small values of the cooperation-range parameter L—larger, however, than the LiF layer thickness—can increase extraction efficiency in comparison to the non-cooperative model. Note also how $L \simeq \frac{\lambda}{4}$ represents a threshold above which the plots reach a stable behavior; this is generally true also for the *total* extraction efficiency, obtained by integrating the powers over the half solid angle in the bottom half space.

5 Conclusions

After a brief review of it, Benisty's theory for SpE by a point source in an optical microcavity [16, 17] has been generalized to a volume source in a layered medium. Three cases have been considered: *(a)* all the points of the volume source radiate in an independent way; *(b)* any point of the volume source cooperates in the SpE process with all the other points of the source (long-range cooperation); *(c)* any point of the volume source cooperates in the SpE process only with those points that are within a certain distance range (short-range cooperation). The peculiarity of the generalized theory is that all the obtained expressions for the radiated power are analytical; they include multi-dimensional Fourier transforms, though. However, such transforms can be analytically evaluated in some selected cases. Several examples have been given in this regard.

As far as the short-range cooperative approach is concerned, the model has been developed on the theory of spatial coherence [32, 34]. The overall emission by a volume source in a layered

[22] As a test, the same curves were calculated for $L \ll \lambda$, that is, in conditions very close to non-cooperation. In this case, by setting, *e.g.*, $L = 1$ nm, the same angular dependencies as in Fig. 13 were recovered.

medium has been evaluated by summing and time-averaging the elementary field contributions of all the source elements, which contain phase terms that randomly vary in time. The time-average takes into account how much distinct elements of the source can cooperate by means of a function, the degree of coherence. This function favors field-summation over intensity-summation for those couples of elements that have a high cooperation level—typically, elements that are within a certain cooperation volume. The dimensions of this volume are model parameters and have to be estimated by other means, *e.g.*, by recurring to cavity quantum electrodynamics. The use of a three-dimensional Gaussian degree of coherence—resembling a Gaussian Shell-model source—has allowed obtaining analytical expressions of the outcoupled powers for some selected shapes of the volume source.

As an application of the theory, the real case of an Alq_3-based OLED has been considered. Two configurations of the device have been analyzed. In the first, the cathode consists of a simple Al layer. In the second, the cathode is replaced with an Al/LiF bi-layer, which was proven to significantly reduce the threshold voltage of the diode [43,44]. The goal was to verify how the presence of the Al/LiF cathode could influence the extraction efficiency of the device by a purely optical point of view. To this purpose, both the non-cooperative and the short-range cooperative models have been applied, finding in both cases that the Al/LiF cathode significantly increases the extraction efficiency of the device: the total extraction efficiency (integrated along all the propagation directions) is increased by 28–33%, while this increase amounts to 42–50% if one limits the observation to the normal direction. Because the intensity-reflection properties of the cathode are practically unaltered by the presence of the LiF layer (Fig. 11), such a better performance is mainly ascribed to the different phase response of the Al/LiF bi-layer in comparison with the Al layer (Fig. 12). Finally, Fig. 15 demonstrates that even better extraction efficiencies could be achieved with a LiF layer thicker than 10 nm, so that the optimum thickness—at least in the considered range—is limited by its convenience in terms of diode threshold voltage.

Acknowledgements

The critical reading of the manuscript and precious suggestions by M. Marrocco are gratefully acknowledged. Research carried out within TECVIM project: *Tecnologie per Sistemi di Visualizzazione di Immagini* (Technologies for Image Visualization Systems) funded by the Italian Ministry of University and Scientific Research MIUR as support to applied research.

A Solid-angle transformation on refraction

Because of refraction, solid angles transform when passing through media with different optical constants [39]. Let us consider two light rays, A and B in Fig. A.1, whose propagation angles are infinitesimally apart. In this figure, we are considering a single interface between two media;

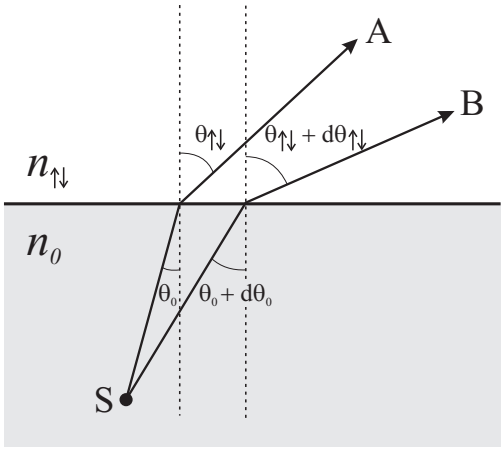

Figure A.1. Transformation of solid angle. The point source, S, emits two light rays, A and B, which undergo refraction when crossing the border between the media of indices n_0 and $n_{\uparrow\downarrow}$.

however, the following results remain valid also if a multilayer is placed between the two media. Because of Snell's law [33], one has

$$n_{\uparrow\downarrow} \sin\theta_{\uparrow\downarrow} = n_0 \sin\theta_0, \qquad n_{\uparrow\downarrow} \sin(\theta_{\uparrow\downarrow} + \mathrm{d}\theta_{\uparrow\downarrow}) = n_0 \sin(\theta_0 + \mathrm{d}\theta_0). \tag{A.1}$$

These two equalities yield

$$n_{\uparrow\downarrow} \cos\theta_{\uparrow\downarrow}\, \mathrm{d}\theta_{\uparrow\downarrow} = n_0 \cos\theta_0\, \mathrm{d}\theta_0. \tag{A.2}$$

In polar coordinates, the infinitesimal solid angles within the two media of Fig. A.1 are

$$\mathrm{d}\Omega_{\uparrow\downarrow} = \sin\theta_{\uparrow\downarrow}\, \mathrm{d}\theta_{\uparrow\downarrow}\, \mathrm{d}\varphi, \qquad \mathrm{d}\Omega_0 = \sin\theta_0\, \mathrm{d}\theta_0\, \mathrm{d}\varphi, \tag{A.3}$$

where the infinitesimal azimuth angle $\mathrm{d}\varphi$ is an invariant on refraction. By putting together all the above relationships, one gets the transformation law for the solid angle,

$$\frac{\mathrm{d}\Omega_0}{\mathrm{d}\Omega_{\uparrow\downarrow}} = \frac{n_{\uparrow\downarrow}^2 \cos\theta_{\uparrow\downarrow}}{n_0^2 \cos\theta_0}. \tag{A.4}$$

The number of photons within any portion of spherical wave that is enclosed within an infinitesimal solid angle is proportional to $w\,\mathrm{d}\Omega$, where w is the radiated power along the observation direction. If T is the intensity transmittance coefficient—for a plane wave—of the interface between the two media in Fig. A.1, then photon balance yields

$$w_{\uparrow\downarrow}\, \mathrm{d}\Omega_{\uparrow\downarrow} = T w_0\, \mathrm{d}\Omega_0, \tag{A.5}$$

while the simpler

$$w_{\uparrow\downarrow} = T w_0 \tag{A.6}$$

holds true for a plane wave. It ensues that, for a spherical wave,

$$w_{\uparrow\downarrow} = \frac{\mathrm{d}\Omega_0}{\mathrm{d}\Omega_{\uparrow\downarrow}}\, T w_0 = \frac{n_{\uparrow\downarrow}^2 \cos\theta_{\uparrow\downarrow}}{n_0^2 \cos\theta_0}\, T w_0. \tag{A.7}$$

Therefore, Eq. (A.4) represents the correction factor needed to adapt to spherical waves the intensity-transmission laws that hold for plane waves.

B Optical pump in the layered medium

Let us consider a monochromatic electromagnetic wave impinging on the layered structure of Fig. 1 with incidence either from the top or bottom medium. For the sake of simplicity, the wave is assumed to be plane. Let $\mathcal{F}^{(h),s}_{\uparrow\downarrow}$, $\mathcal{F}^{(h),p}_{\uparrow\downarrow}$ and $\mathcal{F}^{(v),p}_{\uparrow\downarrow}$ be the components of the electric field *in the external medium*, where $\uparrow$ and $\downarrow$ indicate if the incidence medium is the top or bottom one, respectively, (h) and (v) refer to the component alignment (horizontal and vertical), and s and p stand for the polarization state. One can verify that the corresponding electric-field components injected inside the layer of index n_0 are

$$\mathcal{E}^{(h),s}_{\uparrow\downarrow} = \widetilde{\tau}^{s}_{\uparrow\downarrow} \frac{1+\rho^{s}_{\downarrow\uparrow}}{1-\rho^{s}_{\uparrow}\rho^{s}_{\downarrow}} \mathcal{F}^{(h),s}_{\uparrow\downarrow}, \quad \mathcal{E}^{(h),p}_{\uparrow\downarrow} = \widetilde{\tau}^{p}_{\uparrow\downarrow} \frac{1+\rho^{p}_{\downarrow\uparrow}}{1-\rho^{p}_{\uparrow}\rho^{p}_{\downarrow}} \mathcal{F}^{(h),p}_{\uparrow\downarrow}, \quad \mathcal{E}^{(v),p}_{\uparrow\downarrow} = \widetilde{\tau}^{p}_{\uparrow\downarrow} \frac{1-\rho^{p}_{\downarrow\uparrow}}{1-\rho^{p}_{\uparrow}\rho^{p}_{\downarrow}} \mathcal{F}^{(v),p}_{\uparrow\downarrow}, \quad \text{(B.1)}$$

where the meaning of the ρ and τ symbols is the same as in Sec. 2 (see Eqs. (2.7) and (2.8)); here, however, explicit dependence on polarization has been added and it is understood that these quantities are evaluated at the pump wavelength. As far as the τ symbols are concerned, the tilde over them stresses that incidence from the external medium—that is, reversal of that considered in Sec. 2—has to be taken.

Since the three electric-field components in Eq. (B.1) are orthogonal to each other, the resulting pump intensity within the layer of index n_0 and thickness d is

$$\begin{aligned}
I_{\uparrow\downarrow}(z) &= n_0 \left(\left|\mathcal{E}^{(h),s}_{\uparrow\downarrow}\right|^2 + \left|\mathcal{E}^{(h),p}_{\uparrow\downarrow}\right|^2 + \left|\mathcal{E}^{(v),p}_{\uparrow\downarrow}\right|^2 \right) \\
&= \frac{n_{\uparrow\downarrow}\cos\theta_{\uparrow\downarrow}}{\cos\theta_0} \widetilde{F}^{s}_{\uparrow\downarrow} \left\{ 1 + R^{s}_{\downarrow\uparrow} + 2\sqrt{R^{s}_{\downarrow\uparrow}} \cos\left[kn_0(d \pm 2z)\cos\theta_0 + \phi^{s}_{\downarrow\uparrow} \right] \right\} \left|\mathcal{F}^{(h),s}_{\uparrow\downarrow}\right|^2 \\
&+ \frac{n_{\uparrow\downarrow}\cos\theta_0}{\cos\theta_{\uparrow\downarrow}} \widetilde{F}^{p}_{\uparrow\downarrow} \left\{ 1 + R^{p}_{\downarrow\uparrow} + 2\sqrt{R^{p}_{\downarrow\uparrow}} \cos\left[kn_0(d \pm 2z)\cos\theta_0 + \phi^{p}_{\downarrow\uparrow} \right] \right\} \left|\mathcal{F}^{(h),p}_{\uparrow\downarrow}\right|^2 \\
&+ \frac{n_{\uparrow\downarrow}\cos\theta_0}{\cos\theta_{\uparrow\downarrow}} \widetilde{F}^{p}_{\uparrow\downarrow} \left\{ 1 + R^{p}_{\downarrow\uparrow} - 2\sqrt{R^{p}_{\downarrow\uparrow}} \cos\left[kn_0(d \pm 2z)\cos\theta_0 + \phi^{p}_{\downarrow\uparrow} \right] \right\} \left|\mathcal{F}^{(v),p}_{\uparrow\downarrow}\right|^2, \quad \text{(B.2)}
\end{aligned}$$

where

$$\widetilde{F}^{\sigma}_{\uparrow\downarrow} = \frac{\widetilde{T}^{\sigma}_{\uparrow\downarrow}}{\left| 1 - r^{\sigma}_{\uparrow} r^{\sigma}_{\downarrow} \exp\left(-\mathrm{i}2kn_0 d\cos\theta_0\right) \right|^2} \quad \text{(B.3)}$$

and $\widetilde{T}^{\sigma}_{\uparrow\downarrow}$ is the intensity transmittance for incidence from the external medium of index $n_{\uparrow\downarrow}$ ($\sigma = s, p$). If one assumes normal incidence, Eq. (B.3) simplifies to

$$I_{\uparrow\downarrow}(z) = I_0 \widetilde{F}_{\uparrow\downarrow} \left\{ 1 + R_{\downarrow\uparrow} + 2\sqrt{R_{\downarrow\uparrow}} \cos\left[kn_0(d \pm 2z) + \phi_{\downarrow\uparrow} \right] \right\}, \quad \text{(B.4)}$$

where I_0 is the pump intensity in the external medium. In Eq. (B.4), $\widetilde{F}_{\uparrow\downarrow}$, $R_{\downarrow\uparrow}$ and $\phi_{\downarrow\uparrow}$ are evaluated at $\theta_0 = 0$, and polarization-state labels have been omitted because not applicable to normal incidence.

If N_0 two-energy-level atomic systems are located at $z = z_0$ and I_{sat} is their saturation intensity at the pump wavelength, the number of excited systems is [1]

$$N_{\mathrm{exc}} = N_0 \frac{I_{\uparrow\downarrow}(z_0)}{I_{\mathrm{sat}} + I_{\uparrow\downarrow}(z_0)}, \quad \text{(B.5)}$$

which simplifies to

$$N_{\mathrm{exc}} \approx N_0 \frac{I_{\uparrow\downarrow}(z_0)}{I_{\mathrm{sat}}} \tag{B.6}$$

for pump intensities well below saturation.

References

[1] A. Yariv, *Quantum Electronics*, John Wiley & Sons, New York, 3rd edition, 1987.

[2] P. W. Milonni, *The Quantum Vacuum: an Introduction to Quantum Electrodynamics*, Academic Press, San Diego, 1994.

[3] E. M. Purcell, Spontaneous emission probabilities at radio frequencies, Phys. Rev. **69**, 681 (1946).

[4] P. W. Milonni and P. L. Knight, Spontaneous emission between mirrors, Opt. Commun. **9**, 119–122 (1973).

[5] D. Kleppner, Inhibited spontaneous emission, Phys. Rev. Lett. **47**, 233–236 (1981).

[6] F. De Martini, M. Marrocco, P. Mataloni, L. Crescentini, and R. Loudon, Spontaneous emission in the optical microscopic cavity, Phys. Rev. A **43**, 2480–2497 (1991).

[7] G. Björk, S. Machida, Y. Yamamoto, and K. Igeta, Modification of spontaneous emission rate in planar dielectric microcavity structures, Phys. Rev. A **44**, 669–681 (1991).

[8] T. Baba, T. Hamano, F. Koyama, and K. Iga, Spontaneous emission factor of a microcavity DBR surface-emitting laser, IEEE J. Quantum Electron. **27**, 1347–1358 (1991).

[9] D. G. Deppe and C. Lei, Spontaneous emission from a dipole in a semiconductor microcavity, J. Appl. Phys. **70**, 3443–3448 (1991).

[10] F. De Martini, F. Cairo, P. Mataloni, and F. Verzegnassi, Thresholdless microlaser, Phys. Rev. A **46**, 4220–4233 (1992).

[11] E. F. Schubert, A. M. Vredenberg, N. E. J. Hunt, Y. H. Wong, P. C. Becker, J. M. Poate, D. C. Jacobson, L. C. Feldman, and G. J. Zydzik, Giant enhancement of luminescence intensity in Er-doped Si/SiO_2 resonant cavities, Appl. Phys. Lett. **61**, 1381–1383 (1992).

[12] G. Björk, H. Heitmann, and Y. Yamamoto, Spontaneous-emission coupling factor and mode characteristic of planar dielectric microcavity lasers, Phys. Rev. A **47**, 4451–4463 (1993).

[13] H. Rigneault and S. Monneret, Modal analysis of spontaneous emission in a planar microcavity, Phys. Rev. A **54**, 2356–2368 (1996).

[14] S. Ciancaleoni, P. Mataloni, O. Jedrkiewicz, and F. De Martini, Angular distribution of the spontaneous emission in a planar dielectric dye microcavity, J. Opt. Soc. Am. B **14**, 1556–1563 (1997).

[15] H. Rigneault, S. Robert, C. Begon, B. Jacquier, and P. Moretti, Radiative and guided wave emission of Er^{3+} atoms located in planar multidielectric structures, Phys. Rev. A **55**, 1497–1502 (1997).

[16] H. Benisty, R. Stanley, and M. Mayer, Method of source terms for dipole emission modification in modes of arbitrary planar structures, J. Opt. Soc. Am. A **15**, 1192–1201 (1998).

[17] H. Benisty, H. De Neve, and C. Weisbuch, Impact of planar microcavity effects on light extraction - Part I: Basic concepts and analytical trends, IEEE J. Quantum Electron. **34**, 1612–1631 (1998).

[18] O. Jedrkiewicz and R. Loudon, Theory of transient spontaneous emission by an atom in a planar microcavity, Phys. Rev. A **60**, 4951–4964 (1999).

[19] Y. Xu, R. K. Lee, and A. Yariv, Quantum analysis and the classical analysis of spontaneous emission in a microcavity, Phys. Rev. A **61**, 033807 (2000).

[20] N. Danz, R. Waldhausl, A. Brauer, and R. Kowarschik, Dipole lifetime in stratified media, J. Opt. Soc. Am. B **19**, 412–419 (2002).

[21] N. Danz, J. Heber, and A. Brauer, Fluorescence lifetimes of molecular dye ensembles near interfaces, Phys. Rev. A **66**, 063809 (2002).

[22] R. H. Dicke, Coherence in spontaneous radiation processes, Phys. Rev. **93**, 99–110 (1954).

[23] E. Ressayre and A. Tallet, Basic properties for cooperative emission of radiation, Phys. Rev. Lett. **37**, 424–427 (1976).

[24] H. S. Freedhoff, Spontaneous emission by a fully excited system of three identical atoms, J. Phys. B: At. Mol. Phys. **19**, 3035–3050 (1986).

[25] H. S. Freedhoff, Cooperative spontaneous emission by a fully inverted array of N atoms: small-sample limit, J. Phys. B: At. Mol. Phys. **20**, 285–293 (1987).

[26] F. De Martini, M. Marrocco, and D. Murra, Transverse quantum correlations in the active microscopic cavity, Phys. Rev. Lett. **65**, 1853–1856 (1990).

[27] A. Aiello, F. De Martini, M. Marrocco, and P. Mataloni, Microcavity transverse coherence length and microlaser threshold, Opt. Lett. **20**, 1492–1494 (1995).

[28] Q. Deng and D. G. Deppe, Spontaneous-emission coupling from multiemitters to the quasi-mode of a Fabry-Pérot microcavity, Phys. Rev. A **53**, 1036–1047 (1996).

[29] R. G. DeVoe and R. G. Brewer, Observation of superradiant and subradiant spontaneous emission of two trapped ions, Phys. Rev. Lett. **76**, 2049–2052 (1996).

[30] A. Takada and K. Ujihara, Spontaneous emission by two atoms in a planar microcavity, Opt. Commun. **160**, 146–161 (1999).

[31] J. Eschner, C. Raab, F. Schmidt-Kaler, and R. Blatt, Light interference from single atoms and their mirror images, Nature **413**, 495–498 (2001).

[32] J. W. Goodman, *Statistical Optics*, John Wiley & Sons, New York, 1985.

[33] M. Born and E. Wolf, *Principles of Optics*, Pergamon Press, Oxford, 6th edition, 1987.

[34] L. Mandel and E. Wolf, *Optical coherence and quantum optics*, Cambridge University Press, New York, 1995.

[35] D. S. Citrin, Controlled exciton spontaneous emission in optical-microcavity-embedded quantum wells, IEEE J. Quantum Electron. **30**, 997–1014 (1994).

[36] H. A. Macleod, *Thin-Film Optical Filters*, Macmillan Publishing Company, New York, 2nd edition, 1986.

[37] S. A. Furman and A. V. Tikhonravov, *Basics of Optics of Multilayer Systems*, "Basics of" Series, Editions Frontieres, Paris, 1992.

[38] O. Stenzel, *The Physics of Thin Film Optical Spectra: an Introduction*, volume 44 of *Springer Series in Surface Sciences*, Springer-Verlag, Berlin, 2005.

[39] W. Lukosz and R. E. Kunz, Light emission by magnetic and electric dipoles close to a plane dielectric interface. II. Radiation patterns of perpendicular oriented dipoles, J. Opt. Soc. Am. **67**, 1615–1619 (1977).

[40] M. Marrocco, Coherent anti-Stokes Raman scattering microscopy in the presence of electromagnetic confinement, Laser Phys. **17**, 935–941 (2007).

[41] A. E. Siegman, *Lasers*, University Science Books, Mill Valley, 1986.

[42] G. Baldacchini, S. Gagliardi, S. Gambino, S. Loreti, R. M. Montereali, and A. Pace, Diodi organici luminescenti, Energia, Ambiente e Innovazione **4**, 83–84 (2003).

[43] R. M. Montereali, S. Gambino, S. Loreti, S. Gagliardi, A. Pace, G. Baldacchini, and F. Michelotti, Morphological, electrical and optical properties of organic light-emitting diodes with a LiF/Al cathode and an Al-hydroxyquinoline/diamine junction, Synth. Metals **143**, 171–174 (2004).

[44] T. M. Brown, R. H. Friend, I. S. Millard, D. J. Lacey, J. H. Burroughes, and F. Cacialli, LiF/Al cathodes and the effect of LiF thickness on the device characteristics and built-in potential of polymer light-emitting diodes, Appl. Phys. Lett. **77**, 3096–3098 (2000).

[45] E. D. Palik, *Handbook of Optical Constants of Solids*, Academic Press, London, 1985.

[46] D. Z. Garbuzov, S. R. Forrest, A. G. Tsekoun, P. E. Burrows, V. Bulović, and M. E. Thompson, Organic films deposited on Si p-n junctions: Accurate measurements of fluorescence internal efficiency, and application to luminescent antireflection coatings, J. Appl. Phys. **80**, 4644–4648 (1996).

[47] SPI® Supplies, Online Catalog, `http://www.2spi.com/catalog/standards/ITO-coated-substrates-refractive-index-values.html`.

[48] E. D. Palik, *Handbook of Optical Constants of Solids II*, Academic Press, London, 1991.

Edito dall' ENEA
Funzione Centrale Relazioni Esterne
Unità Comunicazione
Lungotevere Thaon di Revel, 76 - 00196 Roma
www.enea.it
Stampa: Tecnografico ENEA - CR Frascati
Finito di stampare nel mese di marzo 2009